Self-similar mixing in stratified plane Couette flow for varying Prandtl number

Qi Zhou[1,†], John R. Taylor[1] and Colm-cille P. Caulfield[2,1]

[1]Department of Applied Mathematics and Theoretical Physics, University of Cambridge, Wilberforce Road, Cambridge CB3 0WA, UK
[2]BP Institute, University of Cambridge, Madingley Road, Cambridge CB3 0EZ, UK

(Received xx; revised xx; accepted xx)

We investigate fully developed turbulence in stratified plane Couette flows using direct numerical simulations similar to those reported by Deusebio, Caulfield & Taylor (*J. Fluid Mech.*, 781, 2015) expanding the range of Prandtl number Pr examined by two orders of magnitude from 0.7 up to 70. Significant effects of Pr on the heat and momentum fluxes across the channel gap and on the mean temperature and velocity profile are observed. These effects can be described through a mixing length model coupling Monin–Obukhov (M-O) similarity theory and van Driest damping functions. We then employ M-O theory to formulate similarity scalings for various flow diagnostics for the stratified turbulence in the gap interior. The mid-channel-gap gradient Richardson number Ri_g is determined by the length scale ratio h/L, where h is the half channel gap depth and L is the Obukhov length scale. As h/L approaches very large values, Ri_g asymptotes to a maximum characteristic value of approximately 0.2. The buoyancy Reynolds number $Re_b \equiv \varepsilon/(\nu N^2)$, where ε is the dissipation, ν is the kinematic viscosity and N is the buoyancy frequency defined in terms of the local mean density gradient, scales linearly with the length scale ratio $L^+ \equiv L/\delta_\nu$, where δ_ν is the near-wall viscous scale. The flux Richardson number $Ri_f \equiv -B/P$, where B is the buoyancy flux and P is the shear production, is found to be proportional to Ri_g. This then leads to a turbulent Prandtl number $Pr_t \equiv \nu_t/\kappa_t$ of order unity, where ν_t and κ_t are the turbulent viscosity and diffusivity respectively, which is consistent with Reynolds analogy. The turbulent Froude number $Fr_h \equiv \varepsilon/(NU'^2)$, where U' is a turbulent horizontal velocity scale, is found to vary like $Ri_g^{-1/2}$. All these scalings are consistent with our numerical data and appear to be independent of Pr. The classical Osborn model based on turbulent kinetic energy balance in statistically stationary stratified sheared turbulence (*J. Phys. Oceanogr.*, 10, 1980), together with M-O scalings, results in a parameterization of $\kappa_t/\nu \sim \nu_t/\nu \sim Re_b Ri_g/(1-Ri_g)$. With this parameterization validated through direct numerical simulation data, we provide physical interpretations of these results in the context of M-O similarity theory. These results are also discussed and rationalized with respect to other parameterizations in the literature. This paper demonstrates the role of M-O similarity in setting the mixing efficiency of equilibrated constant-flux layers, and the effects of Prandtl number on mixing in wall-bounded stratified turbulent flows.

Key words:

† Email address for correspondence: q.zhou@damtp.cam.ac.uk

1. Introduction

Stratified plane Couette flow is bounded by two horizontal walls moving in opposite directions with a constant velocity. The fluid density at each wall is held at a constant value with a lower density at the upper wall, resulting in a stably stratified system. Stratified plane Couette flow is one of several canonical geometries used to investigate the dynamics of stratified shear flows. Much of the research on stratified plane Couette flow has focused on transition and coherent structures (Deusebio *et al.* 2015; Eaves & Caulfield 2015), turbulent characteristics (García-Villalba *et al.* 2011*a*) and diapycnal mixing (Caulfield *et al.* 2004; Tang *et al.* 2009; García-Villalba *et al.* 2011*b*; Scotti 2015; Deusebio *et al.* 2015). In this paper, we consider the dynamical properties of turbulent stratified plane Couette flow. Our consideration has three main themes: (i) the effects of varying Prandtl number; (ii) the applicability of Monin–Obukhov similarity theory; and (iii) the parameterization of diapycnal mixing in stratified plane Couette flows. Each of the themes is associated with key open questions in the literature.

A stratified plane Couette flow can be characterised by three external parameters: the bulk Reynolds number Re; the bulk Richardson number Ri; and the Prandtl (Schmidt) number $Pr \equiv \nu/\kappa$ (or Sc), where κ is the scalar diffusivity and ν is the kinematic viscosity. While existing stratified plane Couette flow research spans a considerable range of Re and Ri, the Pr (or equivalently Sc) values examined have heretofore been limited to order unity. On the other hand, there has been growing evidence indicating that Pr (or Sc) can indeed have some first-order effects on stratified shear flows. For example, the effects of Pr on the characteristics of secondary instabilities and diapycnal mixing were reported by Salehipour *et al.* (2015) through simulations of growing Kelvin-Helmholtz instabilities. Motivated by these observations, we aim to investigate the effects of variations in Pr systematically in stratified plane Couette flows through direct numerical simulation (DNS), and this investigation constitutes the first theme of this paper.

Stratified plane Couette flows transfer momentum and heat fluxes across the upper and lower walls which provide shear and stratification to the system. In fully developed statistically stationary turbulent stratified plane Couette flows, which are the focus of the present study, the *total* momentum and active scalar fluxes are constant in the wall-normal (vertical) direction y. The very fact that these fluxes are constant in y contrasts stratified plane Couette flows with other wall-bounded flows, such as channel flows (Armenio & Sarkar 2002; García-Villalba & del Álamo 2011; Karimpour & Venayagamoorthy 2014, 2015), where the total momentum flux is maximised at the walls and zero at mid-channel (see e.g. Armenio & Sarkar (2002)). Turner (1973) argued that stably stratified flows may adjust to a tuned vertical flux from rearrangement of the mean flow and scalar profiles, and the turbulent characteristics in such generic constant-flux layers warrant further study.

For decades (see Foken (2006) for a review), the Monin–Obukhov similarity theory has provided a powerful tool to characterise such constant-flux layers. More recently, Monin–Obukhov theory has also been used to interpret stratified turbulence characteristics in homogeneous shear flows (Chung & Matheou 2012). In the context of stratified plane Couette flows, Deusebio *et al.* (2015) demonstrated the usefulness of Monin–Obukhov scaling by delineating the intermittency boundary in (Re, Ri) parameter space at a single Prandtl number $Pr = 0.7$. The Obukhov length scale

$$L \equiv \frac{u_\tau^3}{k_m g \alpha_V q_w}, \tag{1.1}$$

was found to be of dynamical significance in stratified plane Couette flows. Here, u_τ is

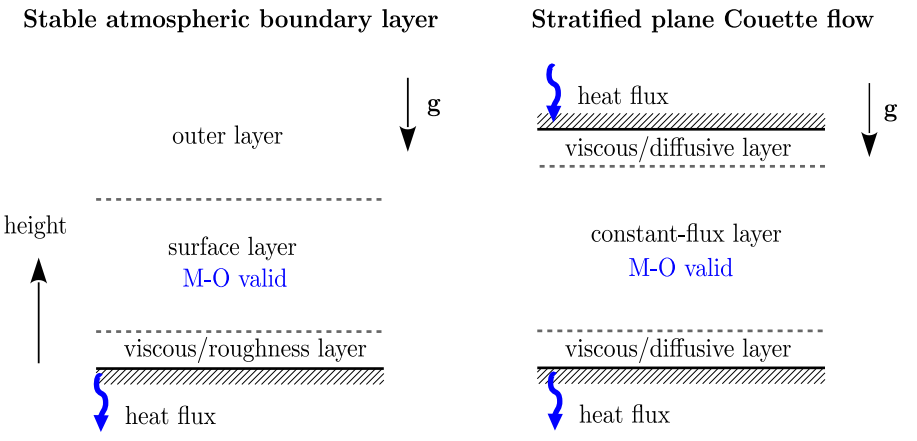

Figure 1: Comparison of a 'weakly stable' atmospheric boundary layer (see e.g. Mahrt (2014)) and a stratified plane Couette flow. The heights of various layers are not drawn to scale.

the friction velocity, k_m is the von Karman constant for momentum, g is gravity, α_V is the thermal expansion coefficient relating fluid temperature θ to density ρ via a linear equation of state

$$\rho = \rho_0(1 - \alpha_V \theta), \tag{1.2}$$

with ρ_0 being the reference density, and q_w is the wall heat flux. The ratio of length scales,

$$L^+ \equiv \frac{L}{\delta_\nu}, \tag{1.3}$$

where $\delta_\nu \equiv \nu/u_\tau$ is the near-wall viscous length scale, needs to be above approximately 200 for a stratified plane Couette flow to stay fully turbulent, while when $L^+ < 200$ the flows become intermittent, i.e. laminar and turbulent flow patches coexist. This observation is consistent with Flores & Riley (2011) who reported similar behaviour in stably stratified boundary layers. Consistent with the L^+ criterion, Deusebio *et al.* (2015) were not able to find fully developed turbulence (see their figure 18) in the SPC system for $Ri > 0.2$ even for Re up to 280000, as the flow inevitably relaminarises due to the strong buoyancy effects, although it is important to appreciate that the simulations had imposed periodicity in the streamwise and spanwise directions, and the extent of the computational domain may play a non-trivial role. Subsequently, Scotti & White (2016) also used Monin–Obukhov similarity theory to consider, among other issues, the mixing properties of stratified plane Couette flow, but they restricted their attention to five simulations at relatively low $Ri \leqslant 0.1$ for $14250 \leqslant Re \leqslant 55000$, using our conventions, and the single value of $Pr = 1$, and so did not consider the parameter regime where this intermittency at high Re for sufficiently high Ri appears to arise.

In this paper, we employ Monin–Obukhov similarity theory to formulate scalings for relevant stratified flow diagnostics in stratified plane Couette flows, which forms the second theme of the paper. It is important to contrast the behaviour of stratified plane Couette flows with the more geophysically realistic flow in a stable atmospheric boundary layer, where the flow is only wall-bounded from below. In stable atmospheric boundary layers, Monin–Obukhov theory is only valid for the 'weakly stable' regime in the surface

layer where the momentum and buoyancy fluxes do not vary with height, as shown in the left panel of figure 1. Monin–Obukhov theory does not apply, for example, in the overlying outer layer, or in the 'very stable' regime where the constant-flux surface layer does not exist (see e.g. Mahrt (2014)). However, in the doubly bounded set-up of stratified plane Couette flows, as shown in the right panel of figure 1, the momentum and buoyancy fluxes do not vary over height under the condition of statistical stationarity, and Monin–Obukhov theory is indeed expected to hold throughout the domain, crucially because the flow is wall-bounded above and below, and so there is a y-independent vertical flux through the domain.

One of the specific goals of the paper is to examine whether stratified plane Couette flow (or any stable constant-flux layer to which Monin–Obukhov scaling applies) supports the strongly stratified turbulence regime (Lilly 1983; Billant & Chomaz 2001; Brethouwer *et al.* 2007; Riley & Lindborg 2012), a regime which requires $Re_b \gg 1$ and $Fr_h \ll 1$, where Re_b is the buoyancy Reynolds number and Fr_h is the horizontal turbulent Froude number. Re_b and Fr_h are defined as

$$Re_b \equiv \frac{\varepsilon}{\nu N^2} \qquad \text{and} \qquad Fr_h \equiv \frac{U'}{N\ell_h}, \tag{1.4}$$

where ε is the dissipation rate, N is the buoyancy frequency, U' is a characteristic turbulent horizontal velocity, and ℓ_h is the horizontal integral scale of the turbulence. Such a strongly stratified regime can be reached numerically in homogeneous and stationary flows with body forcing (Brethouwer *et al.* 2007; de Bruyn Kops 2015), and in unforced nonstationary flows with specific initial conditions (Riley & de Bruyn Kops 2003; Diamessis *et al.* 2011; Zhou 2015; Maffioli & Davidson 2015). However, the existence of the strongly stratified regime has not been reported in wall-bounded stratified flows (García-Villalba *et al.* 2011*a*; García-Villalba & del Álamo 2011; Deusebio *et al.* 2015). Whether this regime is realizable in such flows is a key issue that we investigate in this paper. As demonstrated in Scotti & White (2016), Monin–Obukhov scaling allows the construction of an estimate for Re_b, and so for flows exhibiting Monin–Obukhov scaling there is a convenient theoretical approach to consider the realizability of the strongly stratified regime.

Diapycnal mixing in stratified flows is a focal point of research (see the reviews of Linden (1979); Fernando (1991); Peltier & Caulfield (2003); Ivey *et al.* (2008)). Existing parameterizations of the diapycnal diffusivity κ_t, when normalised by the molecular viscosity ν, often involve Re_b as a parameter (Shih *et al.* 2005; Bouffard & Boegman 2013), although it has been widely debated if Re_b is the *only* parameter of relevance. For example, the additional effects of Ri_g and Pr have been highlighted by laboratory and numerical studies (Barry *et al.* 2001; Mater & Venayagamoorthy 2014; Salehipour & Peltier 2015; Salehipour *et al.* 2015; Maffioli *et al.* 2016; Scotti & White 2016) in parameterizing κ_t, where Ri_g is the gradient Richardson number defined as

$$Ri_g \equiv \frac{N^2}{S^2}, \tag{1.5}$$

with S being an appropriate mean vertical shear. A recent study by Maffioli *et al.* (2016) proposed an alternative scaling based upon the turbulent Froude number Fr_h defined in (1.4). Stratified plane Couette flow is an effective test bed for these parameterizations, as the parameters (Re_b, Ri_g, Pr, Fr_h) can be varied readily by adjusting the external properties (such as wall velocity, density difference, viscosity, etc) in simulations of stratified plane Couette flow. The final theme of this paper is, therefore, to characterize the diapycnal mixing due to stratified turbulence in stratified plane Couette flow at as

large a range of Ri_g, Re_b and Pr as possible and to identify the relevant parameters in determining the turbulent diffusivities in such flows.

In summary, the three main aims of this paper and the corresponding open questions are as follows:

(i) *Prandtl number effects.* For given values of (Re, Ri), how do the mean flow and temperature profiles depend on Pr? How do the wall fluxes of momentum and heat depend on Pr? How does the intermittency boundary in (Re, Ri) parameter space vary with Pr?

(ii) *Similarity scaling.* How well does Monin–Obukhov theory characterise fully developed stratified plane Couette flow? How do diagnosed quantities such as Ri_g, Re_b and Fr_h, arising as outputs of the simulations, relate to the wall fluxes? How do those diagnostics relate to each other? Is the strongly stratified regime accessible in stratified plane Couette flows?

(iii) *Mixing parameterization.* How should one parameterize the turbulent diffusivities in stratified plane Couette flows? Which of the possible parameters (Re_b, Ri_g, Pr, Fr_h) play a role in these flows? Are these parameters independent of each other?

To address these questions, the rest of the paper is structured as follows. In §2 we describe our numerical simulations of stratified plane Couette flows. In §3, we review Monin–Obukhov similarity theory and develop a mixing length model incorporating Monin–Obukhov theory at various Prandtl numbers and applying near-wall corrections (unlike the $Pr = 1$ model presented in Scotti & White (2016) not specifically focussed on stratified plane Couette flow), to predict the wall fluxes in stratified plane Couette flow as a function of external parameters (Re, Ri, Pr). In §4 we present the Prandtl number effects in stratified plane Couette flows through the modification of the near-wall layer and thus the wall fluxes, and explore the implications of these effects for the intermittency boundary in the (Re, Ri) plane. In §5 we employ Monin–Obukhov similarity theory to characterize the turbulence in the channel gap interior and formulate scalings for various flow diagnostics. In §6 we develop parameterizations for turbulent diffusivities in the channel gap interior and discuss the results in the context of Monin–Obukhov scalings presented in §5 and existing parameterizations in the literature. In §7 we provide some concluding remarks.

2. Numerical simulations

In this section we describe DNS of stratified plane Couette flows considered in this paper. These simulations follow closely those of Deusebio *et al.* (2015) (hereinafter referred to as DCT). With a brief summary provided here, we refer the interested reader to DCT for further details on the formulation of the stratified plane Couette simulations. Full descriptions of the DNS algorithms can be found in Taylor (2008) and Bewley (2010).

Consider the velocity vector $\mathbf{u} = (u, v, w)$ in the coordinate system (x, y, z), where x and z are the periodic (horizontal) directions and y the wall-normal (vertical) direction. Two non-slip solid walls, moving in opposite directions in the $x-$direction at velocity $\pm U_w$, are located at $y = \pm h$ respectively. The temperatures θ at the upper and lower walls are fixed at $\pm T_w$ respectively, resulting in a statically stable stratified system. We consider the incompressible Navier-Stokes equations under the Boussinesq approximation

with a linear equation of state as given in (1.2):

$$\frac{\partial \mathbf{u}}{\partial t} + \mathbf{u}\cdot\nabla\mathbf{u} = -\frac{\nabla p}{\rho_0} + \nu\nabla^2\mathbf{u} - \alpha_V\theta\mathbf{g}, \tag{2.1a}$$

$$\frac{\partial \theta}{\partial t} + \mathbf{u}\cdot\nabla\theta = \kappa\nabla^2\theta, \tag{2.1b}$$

$$\nabla\cdot\mathbf{u} = 0\,, \tag{2.1c}$$

where ν and κ are the kinematic viscosity and thermal diffusivity respectively, and $\mathbf{g} \equiv -g\boldsymbol{e}_y$ represents gravity. (It is important to remember that the vertical axis in which gravity acts is denoted by y as is conventional in engineering wall-bounded flow contexts, whereas in geophysical contexts this direction is often denoted by z.)

Stratified plane Couette flows are characterized by three external parameters:

$$Re \equiv \frac{U_w h}{\nu}, \quad Ri \equiv \frac{\alpha_V T_w g h}{U_w^2} \quad \text{and} \quad Pr \equiv \frac{\nu}{\kappa}. \tag{2.2}$$

We denote the mean velocity and temperature by

$$U \equiv \langle u\rangle \quad \text{and} \quad \Theta \equiv \langle\theta\rangle, \tag{2.3}$$

respectively, where $\langle ...\rangle$ represents horizontal averages over the statistically homogeneous x-z plane. The friction velocity u_τ and temperature θ_τ are defined as

$$u_\tau^2 \equiv \frac{\tau_w}{\rho_0} = \nu\left|\frac{\partial U}{\partial y}\right|_{y=\pm h} \quad \text{and} \quad \theta_\tau \equiv \frac{q_w}{u_\tau} \tag{2.4}$$

respectively, where $\tau_w \equiv \rho_0 u_\tau^2$ is the wall shear stress and

$$q_w \equiv \kappa\left|\frac{\partial \Theta}{\partial y}\right|_{y=\pm h} \tag{2.5}$$

is the wall heat flux. The Obukhov length scale L, defined in (1.1), is the only (up to a multiplicative constant) length scale that can be formed using u_τ^2 and q_w, the wall momentum and heat fluxes, along with the buoyancy parameter $g\alpha_V$, where α_V relates temperature to buoyancy via the linear equation of state (1.2). The friction velocity u_τ can be used to form the friction Reynolds number

$$Re_\tau \equiv \frac{u_\tau h}{\nu}, \tag{2.6}$$

and q_w can be made dimensionless to form the Nusselt number

$$Nu \equiv \frac{q_w h}{\kappa T_w} = \frac{h}{T_w}\left|\frac{\partial \Theta}{\partial y}\right|_{y=\pm h}. \tag{2.7}$$

Re_τ and Nu are not known *a priori*, but are rather output parameters which vary with the external parameters (Re, Ri, Pr).

In order to investigate the flow properties as the external parameters vary in the three-dimensional parameter space (Re, Ri, Pr), we first revisit the existing simulations performed by DCT who focused on a fixed $Pr = 0.7$ and varied Re and Ri extensively. A set of simulations performed by DCT at a wide range of Re from 865 to 280000 are reanalysed in the present study, and the parameters covered are listed in Table 1. In addition, new simulations are performed at a fixed Reynolds number $Re = 4250$ for various Pr and Ri. The Re value in the new simulations is large enough to support fully developed turbulence at finite values of Ri, (i.e. there is no observed spatial or

temporal intermittency in the turbulent flow in this geometry) and yet the Re value is small enough to allow, within available computing resources, a parametric study in the (Ri, Pr) parameter space through DNS, which is one of the main aims of this paper.

The input and output parameters of these simulations, both newly performed (simulations 1–12) and reanalysed from the work of DCT (simulations 13–23), are tabulated in Table 1. Pr values spanning two orders of magnitude, i.e. $Pr \in \{0.7, 7, 70\}$, are considered in this paper. The choices of the first two Pr values correspond to the geophysically relevant scenarios of heat (as the active scalar) in air ($Pr = 0.7$) and heat in water ($Pr = 7$) respectively. While the direct geophysical relevance the third examined value of $Pr = 70$ is not immediately apparent, it has been chosen as an intermediate value between 7 and 700, the latter of which corresponds to the relevant Schmidt number Sc of salt in water. Simulation of flows with $Sc = 700$ incurs prohibitive computational costs presently. The $Pr = 70$ simulations are examined in an attempt to probe into the extremely poorly conductive/diffusive regime expected to occur for $Sc = 700$.

In addition to the requirements to resolve the near-wall dynamics adequately, which was described by DCT, the elevated Pr values pose their own requirement on the spatial resolution of the DNS, i.e. to resolve adequately the Batchelor scale of the scalar field ℓ_B (Batchelor 1959), where ℓ_B is defined as

$$\ell_B \equiv \frac{\eta}{Pr^{1/2}}, \tag{2.8}$$

and $\eta \equiv (\nu^3/\varepsilon)^{1/4}$ is the Kolmogorov scale. Equation (2.8) suggests that the grid resolution needs to be approximately tripled when Pr is increased by one order of magnitude, given a fixed η. In setting up our simulations, simulation 3 (which is replicated from DCT's simulation 9 as tabulated in their table 1) with $(Re, Ri, Pr) = (4250, 0.04, 0.7)$, is used as a reference. When Pr is increased from 0.7 (as in DCT's simulations) to 7 (as in our simulations 4–8), the resolution is only doubled. However, grid-independence tests at $Pr = 7$ employing a $384 \times 193 \times 384$ grid yield no significant differences in the turbulence statistics, suggesting that the resolutions of our $Pr = 7$ simulations are sufficient. When Pr is increased from 7 to 70 in simulations 9–12, the resolution is tripled, as required by (2.8).

In stratified plane Couette flow simulations, the size of the computational domain may affect the results when the flow is intermittent, as suggested by DCT. All but one of the new simulations (1–12) performed have horizontal domain dimensions of $(L_x, L_z) = (4\pi h, 2\pi h)$, following the baseline cases adopted by DCT (i.e. simulations 16–22). Due to the constraint of computational resources, however, the simulation of $(Ri, Pr) = (0.04, 70)$ (simulation 9) is performed with the domain dimensions in x and z reduced to 50% of the other simulations, while keeping the same spatial resolution. As reported by DCT, the turbulence statistics are not expected to be sensitive to the domain size if the flow is fully turbulent, which is the case of simulation 9. Throughout this paper, we focus on examining the turbulence characteristics during the statistically stationary phase of the simulations where key statistics such as dU/dy, $d\Theta/dy$ and ε are observed to have reached a steady state. The spatially averaged statistics may fluctuate weakly with time (see DCT's figure 2(b) for example), and the statistics reported in the following are also time-averaged over a time scale of no shorter than $5h/U_w$, i.e. five advective time units, for the simulations with $Pr = 70$. For the simulations with $Pr = 0.7$ and 7, the time-averaging window is typically longer than $50h/U_w$.

Run	Re	Pr	Ri	$(L_x, L_y, L_z)/h$	(N_x, N_y, N_z)	Re_τ	Nu	L^+
1	4250	0.7	0	$(4\pi, 2, 2\pi)$	$(256, 129, 256)$	233	10.6	∞
2	4250	0.7	0.01	$(4\pi, 2, 2\pi)$	$(256, 129, 256)$	215	9.26	2180
3	4250	0.7	0.04	$(4\pi, 2, 2\pi)$	$(256, 129, 256)$	181	6.40	394
4	4250	7	0	$(4\pi, 2, 2\pi)$	$(512, 257, 512)$	233	31.8	∞
5	4250	7	0.01	$(4\pi, 2, 2\pi)$	$(512, 257, 512)$	221	29.7	7660
6	4250	7	0.04	$(4\pi, 2, 2\pi)$	$(512, 257, 512)$	206	25.9	1640
7	4250	7	0.08	$(4\pi, 2, 2\pi)$	$(512, 257, 512)$	180	19.0	653
8	4250	7	0.12	$(4\pi, 2, 2\pi)$	$(512, 257, 512)$	129	8.47	261
9	4250	70	0.04	$(2\pi, 2, \pi)$	$(768, 769, 768)$	231	69.3	9590
10	4250	70	0.16	$(4\pi, 2, 2\pi)$	$(1536, 769, 1536)$	204	50.2	2020
11	4250	70	0.96	$(4\pi, 2, 2\pi)$	$(1536, 769, 1536)$	145	17.0	259
12	4250	70	1.44	$(4\pi, 2, 2\pi)$	$(1536, 769, 1536)$	107	11.2	78.0
13	865	0.7	0.02	$(64\pi, 2, 32\pi)$	$(1024, 65, 1024)$	47	2.17	256
14	2130	0.7	0.04	$(32\pi, 2, 16\pi)$	$(1024, 97, 1024)$	85	2.89	170
15	3925	0.7	0.06	$(16\pi, 2, 8\pi)$	$(768, 129, 768)$	130	3.56	148
16	12650	0.7	0.08	$(4\pi, 2, 2\pi)$	$(512, 161, 512)$	349	7.95	249
17	15000	0.7	0.05	$(4\pi, 2, 2\pi)$	$(768, 257, 768)$	497	13.9	666
18	15000	0.7	0.1	$(4\pi, 2, 2\pi)$	$(512, 193, 512)$	318	5.46	142
19	15600	0.7	0.1	$(4\pi, 2, 2\pi)$	$(512, 193, 512)$	335	5.81	152
20	25000	0.7	0.05	$(4\pi, 2, 2\pi)$	$(768, 385, 768)$	764	20.0	930
21	25000	0.7	0.1	$(4\pi, 2, 2\pi)$	$(768, 257, 768)$	520	8.80	227
22	35000	0.7	0.125	$(4\pi, 2, 2\pi)$	$(768, 289, 768)$	520	6.08	134
23	280000	0.7	0.175	$(2.66, 2, 1.33)$	$(512, 513, 512)$	1578	6.59	117

Table 1: Summary of numerical simulations of stratified plane Couette flows. Simulations 1–12 are performed specifically for the present study with a fixed $Re = 4250$ and varying Pr and Ri, and simulations 13–23 were first reported by Deusebio *et al.* (2015) with a fixed $Pr = 0.7$ and varying Re and Ri. The computational domains are of dimensions (L_x, L_y, L_z), and the number of grid points in each direction is (N_x, N_y, N_z) respectively.

3. First-order closure model

Key quantities in describing stratified plane Couette flows in the framework of Monin–Obukhov similarity theory are the momentum flux u_τ^2 and wall heat flux q_w which are directly linked to the wall gradients via (2.4) and (2.5). It is thus desirable to develop a model to predict the fluxes for varying external parameters. DCT proposed such a model applying Monin–Obukhov theory to the Reynolds-averaged Navier-Stokes equations. However, the model only applied to a single Prandtl number ($Pr = 0.7$). A refined version of the model, which now uses a mixing length formulation to provide a first-order closure for the turbulent fluxes as a function of mean local gradients, is described here. The mixing length specifications are consistent with Monin–Obukhov theory, and near-wall corrections through damping functions (van Driest 1956; Pope 2000) ensure the reliable presentation of the effects of Pr on the wall fluxes.

3.1. *Model formulation*

In order to obtain the vertical profiles of mean velocity and temperature in fully developed turbulent stratified plane Couette flow, we integrate the following set of equations of U and Θ in time (using the laminar profiles as initial conditions) until reaching a steady state:

$$\frac{\partial U}{\partial t} = \nu \frac{\partial^2 U}{\partial y^2} + \frac{\partial}{\partial y}\left(\nu_t \frac{\partial U}{\partial y}\right), \tag{3.1}$$

$$\frac{\partial \Theta}{\partial t} = \kappa \frac{\partial^2 \Theta}{\partial y^2} + \frac{\partial}{\partial y}\left(\kappa_t \frac{\partial \Theta}{\partial y}\right), \tag{3.2}$$

where ν_t and κ_t are the turbulent (eddy) viscosity and diffusivity respectively.

The closure for ν_t in the Reynolds-averaged momentum equation (3.1) can be obtained by specifying a mixing length (see e.g. Pope (2000)):

$$\nu_t = \ell_m^{*2}\left|\frac{\partial U}{\partial y}\right| = \ell_m^* u^*, \tag{3.3}$$

where ℓ_m^* is the mixing length for momentum and the fluctuation velocity

$$u^* = \ell_m^*\left|\frac{\partial U}{\partial y}\right|. \tag{3.4}$$

Similarly, the turbulent flux of scalar in (3.2) can be modelled as

$$-\langle v'\theta'\rangle = \kappa_t \frac{\partial \Theta}{\partial y} = u^*\theta^* = \ell_m^*\left|\frac{\partial U}{\partial y}\right|\ell_s^*\frac{\partial \Theta}{\partial y}, \tag{3.5}$$

where ℓ_s^* is the scalar mixing length, and it follows that

$$\kappa_t = \ell_s^*\ell_m^*\left|\frac{\partial U}{\partial y}\right| = \ell_s^* u^*. \tag{3.6}$$

It remains to specify the two mixing lengths ℓ_m^* and ℓ_s^*.

To do this, we start by considering unstratified flows, i.e. $L \to \infty$. We define y_w as the wall-normal (vertical) distance to the closer wall, i.e. $y_w \equiv \min(h-y, h+y)$. The length y_w can be normalised in wall units as $y^+ \equiv y_w/(\nu/u_\tau)$. The 'law of the wall' of unstratified wall-bounded flows (see e.g. Bradshaw & Huang (1995)) prescribes the wall-normal gradients of U and Θ in the log-law region, i.e. $y^+ > 30$ (Pope 2000), as

$$\frac{\partial U}{\partial y} = \frac{u_\tau}{k_m y_w} \qquad \text{and} \qquad \frac{\partial \Theta}{\partial y} = \frac{\theta_\tau}{k_s y_w} = \frac{\theta_\tau \hat{Pr}_t}{k_m y_w}. \tag{3.7}$$

where k_m and k_s are the von Karman constants for momentum and scalar respectively, and $\hat{Pr}_t = k_m/k_s$ is a turbulent Prandtl number which applies for the log-law region. With

$$u_\tau^2 \cong \nu_t\left|\frac{\partial U}{\partial y}\right| \qquad \text{and} \qquad q_w = \theta_\tau u_\tau \cong \kappa_t\left|\frac{\partial \Theta}{\partial y}\right|, \tag{3.8}$$

in the log-law region and following the model prescriptions in (3.3) and (3.6), the mixing lengths ℓ_m^* and ℓ_s^* corresponding to (3.7) read

$$\ell_m^* = k_m y_w \qquad \text{and} \qquad \ell_s^* = k_s y_w = \ell_m^* \hat{Pr}_t^{-1}. \tag{3.9}$$

As a result, the velocity scale u^* in (3.3) and (3.6) can be specified as

$$u^* = u_\tau. \tag{3.10}$$

When the fluid is stratified, Monin–Obukhov similarity theory prescribes the vertical gradients of U and Θ as

$$\frac{\partial U}{\partial y} = \frac{u_\tau}{k_m y_w}\Phi_m(\xi) \qquad \text{and} \qquad \frac{\partial \Theta}{\partial y} = \frac{\theta_\tau}{k_s y_w}\Phi_s(\xi). \tag{3.11}$$

In these expressions, Φ_m and Φ_s are Monin–Obukhov functions which are linear in the non-dimensional variable $\xi \equiv y_w/L$ for stable stratification:

$$\Phi_m(\xi) = 1 + \beta_m \xi \qquad \text{and} \qquad \Phi_s(\xi) = 1 + \beta_s \xi. \tag{3.12}$$

Here we take $k_m = 0.41$ and $k_s = 0.48$ following Bradshaw & Huang (1995). The choice of $\beta_m = 4.8$ follows the recommendation of Wyngaard (2010) and $\beta_s = 5.6$ is used following the specific choice of k_m and k_s. These model constants are determined empirically using field observations of stable atmospheric boundary layers, and their values can exhibit some uncertainties (see Foken (2006) for a review). The form of the similarity functions may also require additional corrections in order to match the field situations (see e.g. Tastula *et al.* (2015)), such as varying fluxes with height. In the idealised situation considered here, where the entire flow between the walls is a constant-flux layer by construction, we use the classical canonical forms of Monin–Obukhov functions described in (3.12) for clarity and simplicity.

The mixing length formulation corresponding to Monin–Obukhov theory becomes

$$\ell_m^* = k_m y_w \Phi_m^{-1}(\xi) \qquad \text{and} \qquad \ell_s^* = k_s y_w \Phi_s^{-1}(\xi). \tag{3.13}$$

Taking $\xi \to 0$ in (3.13), one recovers the unstratified formulation (3.9). Since ℓ_m^* and ℓ_s^* are specified in (3.13) in very similar ways, the ratio ℓ_m^*/ℓ_s^* is expected to be of order unity.

3.2. *The near-wall layer*

Here we focus on the viscous wall region, i.e. $y^+ < 50$ (Pope 2000), where the (molecular) Prandtl number Pr plays a critical role. The mean velocity and temperature differences relative to the closer wall can be written in wall units as

$$U^+ = \frac{\min(U + U_w, U_w - U)}{u_\tau} \qquad \text{and} \qquad \Theta^+ = \frac{\min(\Theta + T_w, T_w - \Theta)}{\theta_\tau}, \tag{3.14}$$

where the velocity and temperature at the upper and lower walls are fixed at $\pm U_w$ and $\pm T_w$, respectively. In the viscous/conductive sublayer near the wall (as shown in figure 2 for Θ^+),

$$U^+ = y^+ \qquad \text{and} \qquad \Theta^+ = y^+ Pr. \tag{3.15}$$

As y^+ increases, the viscous/conductive sublayer transitions into the log-law region for which the mean profiles can be obtained by integrating (3.7) to yield

$$U^+ = \frac{1}{k_m}\ln y^+ + C_m \qquad \text{and} \qquad \Theta^+ = \frac{1}{k_s}\ln y^+ + C_s = \frac{\hat{Pr}_t}{k_m}\ln y^+ + C_s. \tag{3.16}$$

DNS of stratified plane Couette flows recover such behaviour in the near-wall region, as shown in figure 2. Unlike C_m which is a constant (we take $C_m = 5.0$ following Bradshaw & Huang (1995)), C_s is thought to be a function of Pr, e.g. following Schlichting & Gersten (2003),

$$C_s = 13.7 Pr^{2/3} - 7.5, \tag{3.17}$$

or following Davidson (2004),

$$C_s = 1.67(3Pr^{1/3} - 1)^2. \tag{3.18}$$

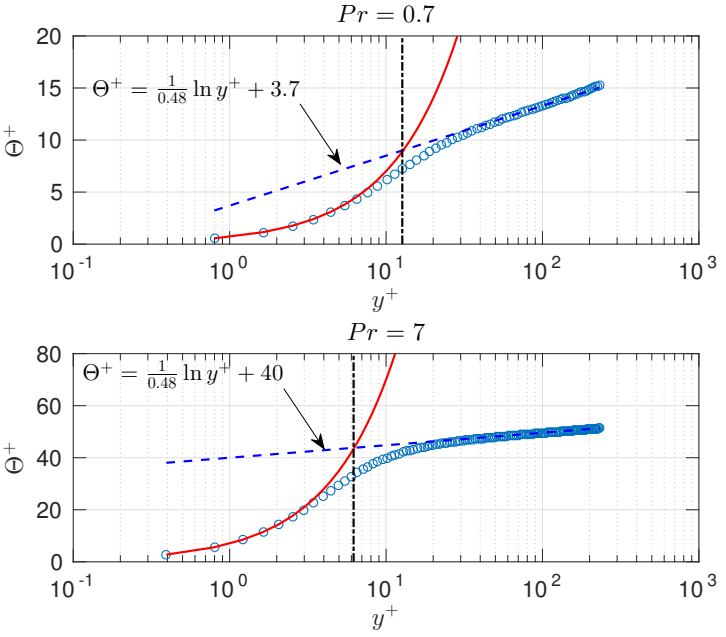

Figure 2: Normalized temperature difference from the wall value, Θ^+ as defined in (3.14), plotted as a function of normalized wall distance y^+. Upper panel: $Pr = 0.7, Ri = 0$ (simulation 1); lower panel: $Pr = 7, Ri = 0$ (simulation 4). Circles show DNS data; the conductive law (3.15) is plotted with a solid line; the logarithmic law (3.16) in which the additive constant C_s varies with Pr, is plotted with a dashed line; and the dot-dashed line shows the location of $y^+ = \Delta y^+$, where Δy^+ marks the characteristic height of the conductive sublayer as defined in (3.19).

Figure 2 confirms such an effect of Pr on the log-law layer. The empirical estimates of C_s as a function of Pr, i.e. (3.17) and (3.18), agree well with DNS, as shown in figure 3.

The value of C_s effectively determines the height of the conductive sublayer which can be measured by Δy^+ (as marked with vertical dot-dashed lines in figure 2), the intersect of the conductive law (3.15) and the log law (3.16), i.e.

$$\Delta y^+ Pr = \frac{1}{k_s} \ln \Delta y^+ + C_s(Pr). \tag{3.19}$$

The quantity Δy^+ is observed to decrease with Pr (see figures 2 and 3), and, in particular, for $Pr \gg 1$ (Davidson 2004),

$$\Delta y^+ \propto Pr^{-1/3}. \tag{3.20}$$

With (3.15), the temperature difference across the conductive sublayer, i.e.

$$\Delta\Theta^+ \sim Pr \Delta y^+ \propto Pr^{2/3}, \tag{3.21}$$

varies strongly with Pr.

It is thus shown that Pr has a significant effect on the near-wall structure of the mean scalar field. A thinner conductive layer is expected at higher values of Pr, as suggested by (3.20). Moreover, as the temperature gradients (in wall units) are sharper at a larger Pr, as quantified by (3.15), the temperature jump across the conductive sublayer increases with Pr, as quantified by (3.21). This generic behaviour of the 'law of the wall' for varying

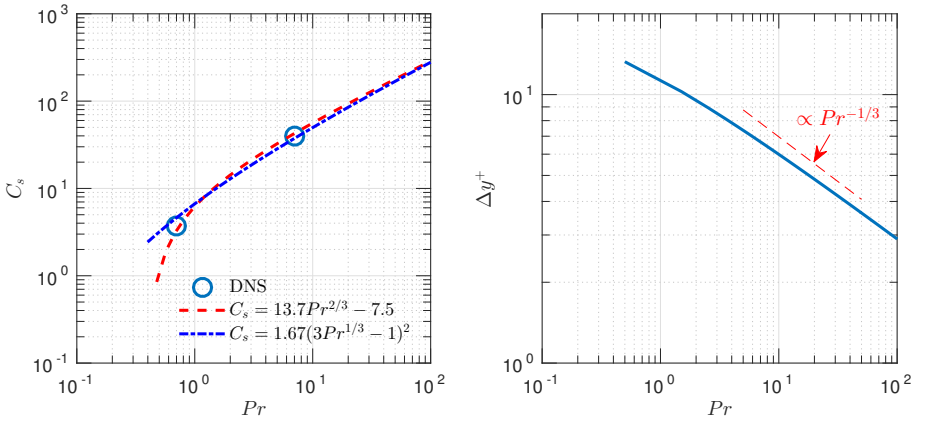

Figure 3: Effect of Pr on the near-wall layer. Left panel: Variation with Pr of the additive constant C_s in the log law for scalar (3.16) as determined by simulations 1 and 4 of stratified plane Couette flows and empirical relations (3.17) and (3.18). Right panel: The height of the conductive sublayer Δy^+ as a function of Pr. Δy^+ values obtained by solving (3.19) and (3.17) are plotted with a solid line, while the dashed line shows the scaling $\Delta y^+ \propto Pr^{-1/3}$.

Pr has implications for the overall temperature profile across the channel gap in stratified plane Couette flows, as we discuss in detail in §4.

3.3. *Damping functions*

To complete the mixing length specifications by taking into account the near-wall layer and the effect of Pr mentioned above, one can apply the van Driest damping functions (van Driest 1956) to the mixing lengths in (3.13). This near-wall correction improves the modelling of the turbulent fluxes in terms of their dependence on y_w in the viscous/conductive sublayer (Pope 2000). The momentum mixing length is corrected by the damping function $\mathrm{D}_m(y^+)$ to become

$$\ell_m^* = k_m y_w \Phi_m^{-1}(\xi)\mathrm{D}_m(y^+) = k_m y_w \Phi_m^{-1}(\xi)[1 - \exp(-y^+/A_m^+)], \tag{3.22}$$

where the van Driest constant for momentum A_m^+ is set to be 26 (van Driest 1956; Pope 2000).

Similarly, the scalar mixing length becomes

$$\ell_s^* = k_s y_w \Phi_s^{-1}(\xi)\mathrm{D}_s(y^+) = k_s y_w \Phi_s^{-1}(\xi)[1 - \exp(-Pr^{-1}y^+/A_s^+)], \tag{3.23}$$

where the constant A_s^+ is inherently related to the Pr-dependent additive constant C_s in (3.16) (Pope 2000) and is thus also a function of Pr.

As $y^+ \to 0$, the turbulent diffusivity κ_t in the conductive sublayer, following (3.23), scales as

$$\kappa_t = \ell_s^* u^* = \ell_s^* \ell_m^* |\frac{dU}{dy}| \sim k_s k_m \frac{y^{+4}}{A_s^+ A_m^+}\frac{\nu}{Pr} \sim k_s k_m \frac{y^{+4}}{A_s^+ A_m^+}\kappa. \tag{3.24}$$

Note that (3.24) does not yield the expected power law, i.e. $\kappa_t \propto y^3$, that describes the near-wall variation of κ_t, which is a shortcoming of the van Driest model (see Pope (2000), pg 305). We use the standard van Driest model for its simplicity. More sophisticated near-wall treatments for large Prandtl (Schmidt) number can be found in e.g. van Reeuwijk

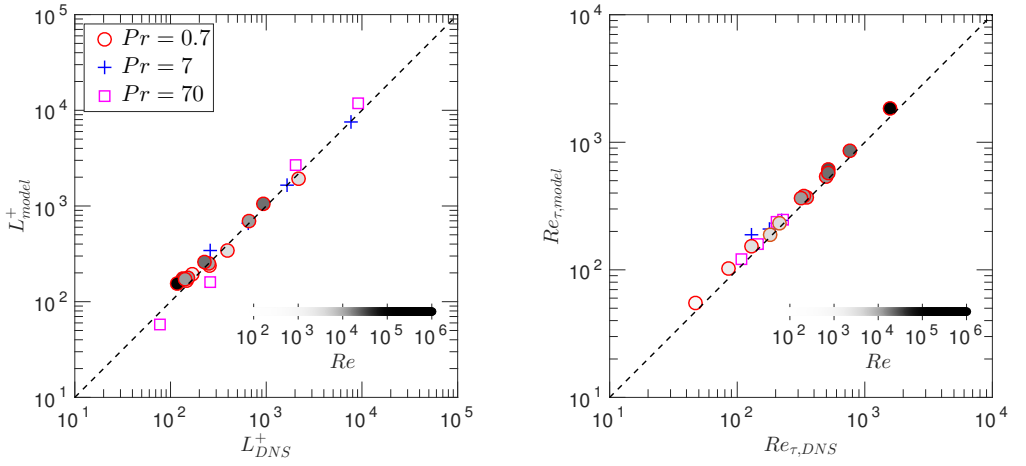

Figure 4: Comparison of the model prediction of L^+ and Re_τ with DNS data from the present study and Deusebio *et al.* (2015). L^+_{model} and $Re_{\tau,\text{model}}$ are the results of the mixing length model as described in §3; L^+_{DNS} and $Re_{\tau,\text{DNS}}$ are the results of DNS which are tabulated in Table 1. Varying Reynolds numbers are used in the simulations with $Pr = 0.7$ (plotted with circles) and the fill colour is made darker for larger values of Re.

& Hadžiabdić (2015). The inclusion of Pr^{-1} in the scalar damping function $\mathrm{D}_s(y^+)$ in (3.23) is such that κ_t in the near-wall limit is proportional to the molecular diffusivity κ (rather than $\nu = \kappa Pr$).

The quantity A_s^+ is, by definition, a dimensionless wall distance below which the damping takes place. A natural choice for A_s^+ is to take $A_s^+ \sim \Delta y^+$ where the latter is a characteristic height of the conductive sublayer as defined by (3.19). In this model, we take $A_s^+ = 0.65\Delta y^+$. This results in A_s^+ values of $\{7.9, 4.3, 2.1\}$ respectively for $Pr \in \{0.7, 7, 70\}$.

3.4. *Comparisons with DNS*

This Monin–Obukhov mixing length model as described above can be implemented to produce predictions of wall fluxes u_τ^2 and q_w and the dimensionless parameters defined in terms of the various fluxes, given the external parameters Re, Ri and Pr. Figure 4 shows the comparisons between the model predictions of $L^+ \equiv L/\delta_\nu$ and $Re_\tau \equiv h/\delta_\nu$ (see definitions in (1.3) & (2.6) respectively) and DNS results at $Re = 4250$ (the present study) and a (crucially) wider range of Re values (Deusebio *et al.* 2015) as listed in table 1. Given the considerable range of parameters, the agreement of the model predictions with DNS data is reasonable, with the L_2 norm of percentage relative errors being 16.4% for L^+ and 13.9% for Re_τ over all simulations tested in figure 4. We believe that the model is thus validated and can be employed to produce an estimate of the wall fluxes given the (externally set) (Re, Ri, Pr) parameters.

4. Effects of Prandtl number

In this section, we examine the DNS results focusing on the effects of the Prandtl number Pr, which is the first main theme of this paper. In particular, we will address the three main questions already posed in the Introduction: i) how does Pr modify the mean flow/temperature profiles; ii) what do these modifications imply for the momentum and

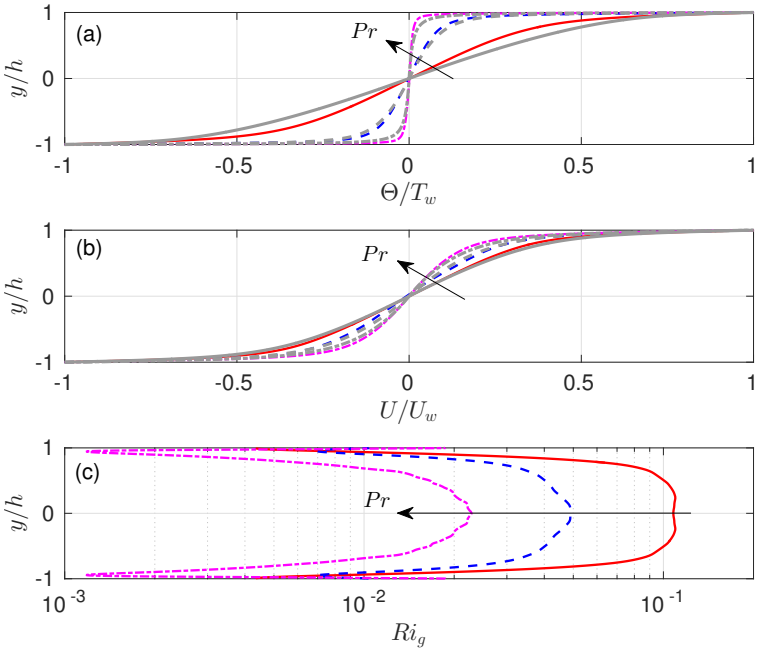

Figure 5: Vertical profiles of: (a) mean temperature Θ/T_w; (b) mean velocity U/U_w; and (c) gradient Richardson number Ri_g at $(Re, Ri) = (4250, 0.04)$. The results of simulation 3 with $Pr = 0.7$ are plotted with a solid line; the results of simulation 6 with $Pr = 7$ are plotted with a dashed line; and the results of simulation 9 with $Pr = 70$ are plotted with a dot-dashed line. For reference, in panels a & b, grey lines with the corresponding line type for each Pr show the predictions of the mixing length model described in §3.

heat fluxes through the wall; and iii) how does the intermittency boundary, delineated in the (Re, Ri) space, vary with Pr?

Figure 5 shows the effects of Pr on the mean velocity (U) and mean temperature (Θ) profiles in the wall-normal y-direction. At fixed values of $(Re, Ri) = (4250, 0.04)$, the mean temperature gradient $d\Theta/dy$ (plotted in figure 5(a)) sharpens significantly in the near-wall region, as Pr increases by two orders of magnitudes from 0.7 to 70. On the other hand, the vertical variation of Θ weakens in the interior of the channel gap away from the walls with increasing values of Pr. The gradient Richardson number (plotted in figure 5(c)), is defined as

$$Ri_g(y) \equiv \frac{N^2}{S^2} = \frac{-(g/\rho_0)(d\overline{\rho}/dy)}{(dU/dy)^2} = \frac{g\alpha_V(d\Theta/dy)}{(dU/dy)^2}, \tag{4.1}$$

where $S \equiv dU/dy$ denotes the mean vertical shear and U is the mean velocity as defined in (2.3). Ri_g varies sharply in the near-wall region and reaches a plateau in the channel gap interior. Given that the mean shear S (plotted in figure 5(b)) is less sensitive to Pr, the Ri_g values at mid-gap $(y = 0)$ decrease with Pr at fixed values of (Re, Ri), which is mainly attributed to the sharpening of $d\Theta/dy$ in the near-wall region and weakening of those gradients (and thus the strength of stratification, as measured by N^2) in the channel gap interior.

We now examine the effects of Pr on Nu, Re_τ and L^+, dimensionless quantities which are determined by the wall fluxes of heat and momentum. As shown by DCT, critical to

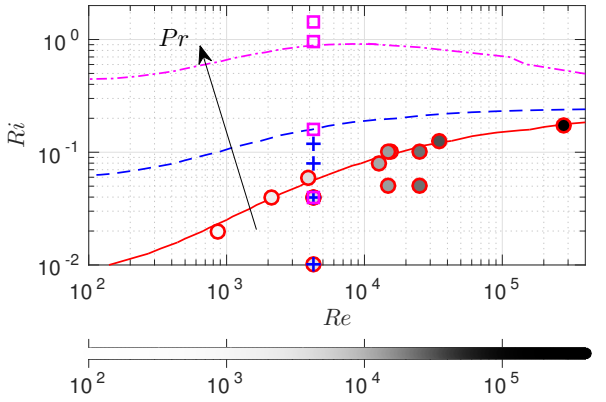

Figure 6: Effect of Pr on the intermittency boundary on the (Re, Ri) plane. Contours corresponding to $L^+ = 200$, the minimum L^+ value for fully developed turbulence (no intermittency) as proposed by DCT, are constructed using the mixing length model described in §3. The areas corresponding to $L^+ > 200$ are *below* the various contour line, plotted with a solid line for $Pr = 0.7$, with a dashed line for $Pr = 7$ and with a dot-dashed line for $Pr = 70$. The (Re, Ri) combinations for the simulations (see table 1) considered in the present study are marked with circles for $Pr = 0.7$, with pluses for $Pr = 7$ and with squares for $Pr = 70$. Varying Reynolds numbers are used in the simulations at $Pr = 0.7$, and the fill colour in the circles is made darker for larger values of Re to match figure 4.

the transition from intermittent behaviour to fully turbulent behaviour is the parameter L^+, which can be rewritten in terms of the bulk input external parameters (Re, Ri, Pr) and the output parameters (Re_τ, Nu) as

$$L^+ = \left(\frac{1}{k_m Re^2 Ri}\right)\left(\frac{Re_\tau^4}{Nu/Pr}\right). \tag{4.2}$$

Consider the scenario where (Re, Ri) are fixed and Pr is adjusted by varying κ. The first bracket on the right hand side of (4.2) is thus fixed, and the second bracket includes all parameters that are Pr-dependent. The term Re_τ^4 is a measure of momentum flux (shear stress), and the term $Nu/Pr = q_w h/(T_w \nu)$ quantifies the stabilizing effect of stratification. By inspecting the values of Re_τ and Nu in table 1 as they vary with Pr, (in particular, simulations 3, 6 and 9 which share the same (Re, Ri)) it appears that Re_τ increases and Nu/Pr decreases as Pr increases. In combination, these two effects result in larger values of L^+. Therefore, at given (Re, Ri) values, larger Pr enhances the destabilizing wall shear stress and inhibits the stabilizing heat flux. The flow thus becomes more prone to turbulence due to the increase of Pr.

Figure 6 demonstrates the effect of Pr on the intermittency boundary dividing the fully turbulent flow regime from the intermittent regime. Contours corresponding to $L^+ = 200$, i.e. the intermittency boundary proposed by DCT, are plotted on the (Re, Ri) plane. At a given Re, increasing Pr effectively allows fully turbulent flows to exist at higher values of Ri. This can be understood from two perspectives. First, as discussed previously, increasing Pr destabilizes the flow due to the combined effects of larger shear and smaller stratification. Second, Pr reshapes the mean temperature and velocity profiles which results in smaller gradient Richardson number Ri_g values in the channel gap interior as

Pr increases (as shown in figure 5) allowing shear to dominate stratification away from the walls. While large values of Pr can raise the transitional Ri value for a given Re, figure 6 suggests that fully developed turbulence is not likely to exist for $Ri \gg 1$, at least within the range of Re and Pr values which has been investigated, both for the simulations conducted specifically for this paper at $Re = 4250$, and the simulations at a range of Re presented by DCT, as listed in table 1.

5. Monin–Obukhov similarity scaling

It has been shown in §4 that Pr plays a significant role in the *near-wall* region by modulating the wall heat flux q_w, the momentum flux u_τ^2 and thus the dimensionless parameters such as L^+ and Re_τ. In this section, we turn our attention to our second main theme, i.e. assessing the validity of Monin–Obukhov similarity scaling. We focus on the turbulence in the *interior* of the channel gap and examine how the turbulence characteristics relate to the wall fluxes q_w and u_τ^2. Scalings for various flow diagnostics are formulated in the context of Monin–Obukhov theory (see details in appendices A and B, and the similar formulations considered independently by Scotti & White (2016)). These predictions are then compared to DNS data shown in figure 7 and the dynamical implications of these scalings are discussed in detail in this section. Simulations specifically performed for the present study, i.e. simulations 1–12 as listed in table 1, which cover a wide range of Pr, as well as those performed by DCT, i.e. simulations 13–23, which cover a wide range of Re, are included in our discussions.

5.1. *Equilibrium Richardson number*

We first revisit the mid-gap gradient Richardson number $Ri_g|_{y=0}$ for fully developed stationary (equilibrium) stratified plane Couette flows as prescribed by Monin–Obukhov scaling. The concept of just such a characteristic equilibrium Ri_g value was discussed by Turner (1973) in the context of constant flux layers. There also exists a large body of literature considering the 'stationary Richardson number' in homogeneous sheared stratified turbulence, e.g. see Shih *et al.* (2000), where the particular value of the gradient Richardson number is imposed by construction, and the references therein. A more recent discussion by Galperin *et al.* (2007) questioned whether such a unique 'critical Richardson number' exists, although the flows considered there differed in several significant ways from the flows considered here. Specifically, and most importantly, stratified plane Couette flow exhibits intermittency for the bulk Richardson number $Ri \lesssim O(1)$. Also, as we discuss in more detail below, the turbulent Prandtl number, i.e. the ratio of eddy diffusivities of heat and momentum, behaves in a qualitatively different manner in stratified plane Couette flow from the behaviour of the 'quasi-normal scale elimination' (QNSE) model used in Galperin *et al.* (2007). Under the plausible assumption that a critical Richardson number exists at least in the flow geometry under consideration here, it may help us to assess if the turbulence would be self-sustained if the externally imposed Richardson number matches the equilibrium condition, or if the flow would self-adjust under the non-equilibrium conditions (Turner 1973). Examples of the adjustment in the latter scenario include the formation of 'layer' and 'interface' structures through the rearrangement of velocity and density profiles so that the equilibrium Richardson number is maintained everywhere in the vertical direction (see §10, Turner (1973)).

Figure 7(a) compares the mid-gap equilibrium $Ri_g|_{y=0}$ values from DNS data (from both the present study and those by DCT crucially at a range of Re) with the model

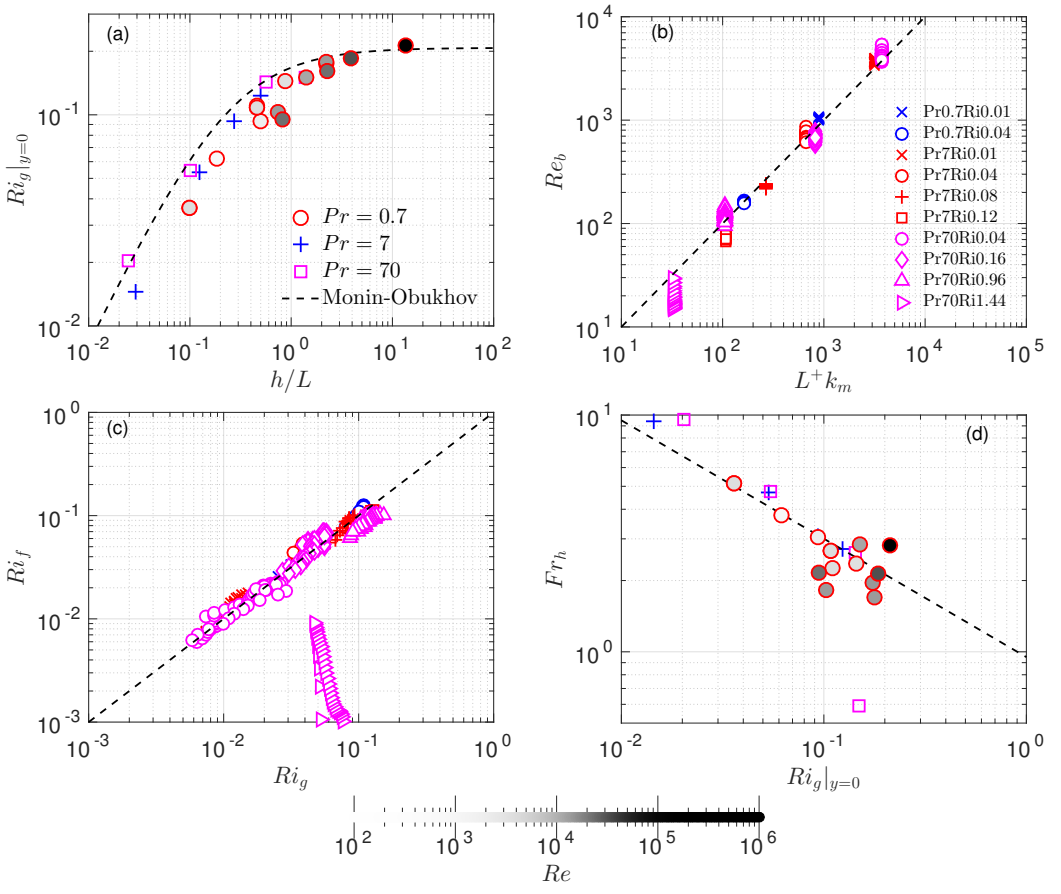

Figure 7: DNS verification of the Monin–Obukhov scalings (5.1), (5.3), (5.4) and (5.7). (*a*) Equilibrium gradient Richardson number $Ri_g|_{y=0}$ at mid-gap, as a function of length scale ratio h/L. (*b*) Buoyancy Reynolds number Re_b as a function of length scale ratio L^+. Re_b values are computed pointwise in y for the channel gap interior with $y^+ > 50$. (*c*) Flux Richardson number $Ri_f \equiv -B/P$ as a function of gradient Richardson number Ri_g. Ri_f and Ri_g values are computed pointwise in y in the channel gap interior with $y^+ > 50$. Symbol types are the same as panel *b*. (*d*) Turbulent Froude number Fr_h as a function of mid-gap gradient Richardson number Ri_g. Fr_h is estimated as $\varepsilon/(Nu_\tau^2)$, where ε and N are sampled at mid-gap $y = 0$. Symbol types are the same as in panel *a*. The dashed line corresponds to $Fr_h = 0.95Ri_g^{-1/2}$, the least-squares fit to the scaling (5.7). In panels *a* & *d*, the fill colours of the circles (corresponding to simulations with $Pr = 0.7$) are made darker for larger values of Re.

prediction (B 3) derived in appendix B, i.e.

$$Ri_g|_{y=0} = \frac{k_m}{k_s}\frac{(h/L)^{-1} + \beta_s}{\left[(h/L)^{-1} + \beta_m\right]^2}, \tag{5.1}$$

which suggests that such an equilibrium Ri_g value is determined solely by the length scale ratio h/L (note that k_m, k_s, β_s and β_m are model constants defined in §3). The data points indeed collapse in figure 7(a) for the wide range of external parameters (in

particular, Prandtl number Pr, but also Reynolds number Re) examined, and the DNS results compare well with the Monin–Obukhov prediction (5.1).

Two scenarios in stratified plane Couette flows arise from (5.1) when h/L approaches different limits. First, when $h/L \to \infty$, the mid-gap equilibrium Ri_g saturates at

$$Ri_g|_{y=0} = \frac{k_m}{k_s}\frac{\beta_s}{\beta_m^2} \simeq 0.21. \tag{5.2}$$

This scenario is at least superficially similar to the discussion of constant-flux layers in 'very stable' stratification (Ellison 1957; Turner 1973), although as discussed further below, the behaviour of the turbulent Prandtl number is qualitatively different from that assumed by Ellison (1957). When $\xi = h/L \gg 1$, the *linear* dependence of Monin–Obukhov functions Φ_m and Φ_s on ξ dominates (see (3.11) and (3.12)). Fluid in the channel gap interior does not 'feel' the impact of the wall directly (but still indirectly though the wall fluxes u_τ^2 and q_w), because the vertical motions are strongly damped by stratification. In the channel gap interior, the distance to the wall y_w (or the channel gap half-height h) becomes irrelevant, as shear and temperature gradients both become constant (by taking the limit of (3.12) at $\xi \to \infty$), which renders the turbulence close to homogeneous in the wall-normal direction. Interestingly, the *maximum* stationary Ri_g reported in homogeneous sheared turbulence is also approximately 0.2 (see e.g. Shih *et al.* (2000)). This reinforces the notion that Monin–Obukhov scaling may also apply to such homogeneous triply-periodic flows (Chung & Matheou 2012). There remains some debate as to whether the standard Monin–Obukhov theory holds in the $\xi \to \infty$ limit in a stable atmospheric boundary layer, see for example the discussion on 'z-less' stratification by Mahrt (1999), and any such differences between the standard theory and boundary layer flow are likely linked to the variation of fluxes with height in a real boundary layer. However, the statistically stationary stratified plane Couette flows examined here, which are constant-flux layers by construction, appear to be consistent with the standard Monin–Obukhov theory.

As an aside, we note that this maximum observed Richardson number is close to $Ri_g = 1/4$ which arises in the well-known Miles–Howard criterion for linear normal mode stability of inviscid parallel steady stratified shear flows (Miles 1961; Howard 1961). This closeness is apparently fortuitous, as the arguments leading to the prediction of the value in (5.2) are entirely constructed under the assumption of statistically stationary turbulent flow. Therefore, it is at least possible that observations of Ri_g close to $1/4$, as, for example, in the Equatorial Undercurrent (Smyth & Moum 2013), are due to turbulent balances, not 'marginal stability' of the flow, as argued by Thorpe & Liu (2009), although, it is also important to remember, as shown for example by Pham *et al.* (2013), that the dynamics of the Equatorial Undercurrent is inevitably non-stationary, due to diurnal forcing.

Second, when h/L is $O(1)$ or smaller, the equilibrium Ri_g at mid-gap varies strongly with h/L, which can be seen from figure 7(a). Under this scenario, the stabilising effects due to stratification are relatively weak. The direct influence of the walls on the interior turbulence becomes significant, and both h and L become relevant scales for the channel gap interior.

5.2. L^+, Re_b and intermittency

The parameter L^+ is a useful diagnostic quantity to predict if stratified plane Couette flows can sustain a fully turbulent state or become intermittent (as discussed by DCT). On the other hand, the buoyancy Reynolds number $Re_b \equiv \varepsilon/(\nu N^2) \sim (\ell_O/\eta)^{4/3}$, which describes the scale separation between the Ozmidov scale ℓ_O and the Kolmogorov scale η, is often used to predict whether small scale turbulence can exist given the level of

turbulent dissipation and stratification (see e.g. Riley & Lindborg (2012)), typically in homogeneous simulations (Brethouwer *et al.* 2007).

A natural question to ask is then whether L^+ and Re_b are related to each other, at least in stratified plane Couette flows. The analysis in Appendix B has, through Monin–Obukhov similarity theory, predicted a linear scaling between L^+ and Re_b as given by (B 5) shown in Appendix B, i.e.

$$Re_b \sim L^+ k_m. \tag{5.3}$$

In figure 7(b) this scaling is confirmed from DNS data (shown for simulations 1–12), and has already been noted by Scotti & White (2016) in a more limited range of $Ri \leqslant 0.1$, $Re \leqslant 55000$ and $Pr = 1$. Re_b estimates presented here are based on ε and N values that are sampled pointwise in the vertical direction y. However, in open flows, there are different possible choices of averaging volumes for ε and N (see e.g. Salehipour *et al.* (2016)), and caution needs to be exercised when comparing specific numerical values of Re_b between different flow geometries, or indeed between different analyses. A reanalysis of DCT's data (simulations 13–23, not shown) suggests the same linear scaling for a wide range of Re and Ri. This indicates that the L^+ criterion for predicting intermittency, which is specific to wall-bounded flows, is also linked to this more general Re_b argument. The critical (minimum) Re_b for fully developed turbulence, as inferred from the $L^+ > 200$ criterion reported by DCT and the scaling (5.3), is approximately 80 (as $k_m \approx 0.4$) for stratified plane Couette flows. This critical Re_b of 80 is close to the cut-off value $Re_b = 100$ between the 'intermediate' and 'energetic' regimes of Shih *et al.* (2005) which is discussed in detail in §6, although one needs to be careful about whether the Re_b value is a 'bulk' or local estimate when comparing the numerical values. Here simulation 12 is in the intermediate regime ($Re_b < 35$, see figure 7(b)), and in what follows, we focus instead on the other simulations ($Re_b > 60$) which are close to or within this 'energetic' regime in terms of the Re_b value.

5.3. *Turbulent Prandtl number*

In appendix B, it is shown through scaling arguments that the flux Richardson number Ri_f is proportional to Ri_g. The particular scaling derived in Appendix B is given by (B 7) i.e.

$$Ri_f \sim Ri_g, \tag{5.4}$$

and is compared to DNS results (simulations 1–12) in figure 7(c). In general, Ri_f is proportional to Ri_g with a multiplicative constant of approximately unity, which is consistent with DCT. The group of points which appear to be outliers, correspond to simulation 12 ($Pr = 70, Ri = 1.44$). As discussed previously, the atypical behaviour associated with this simulation is likely to be due to low-Re_b, and hence inherently viscously dominated effects.

With the turbulent viscosity ν_t defined through the flux-gradient relation

$$\nu_t \equiv -\frac{\langle u'v' \rangle}{S}, \tag{5.5}$$

and turbulent diffusivity κ_t defined in (A 5), the turbulent Prandtl number $Pr_t \equiv \nu_t/\kappa_t$ can be expressed as

$$Pr_t = \frac{Ri_g}{Ri_f}. \tag{5.6}$$

The $Ri_f \simeq Ri_g$ scaling can thus be interpreted alternatively as the turbulent Prandtl number Pr_t being approximately unity, which is consistent with the Reynolds analogy,

as noted independently by Scotti & White (2016). This result can be derived from Monin–Obukhov theory (appendix B) and is consistent with DNS data for the present study (simulations 1–12) shown in figure 7(c)), as well as from revisited DCT datasets (simulations 13–23) which exhibit the same behaviour (not shown).

Pr_t is often parameterized as a function of Ri_g in the literature (see, for example, Venayagamoorthy & Stretch (2010)). Pr_t being unity, as we observe in stratified plane Couette flows (see figure 7(c)), appears to be typical for gradient Richardson numbers $Ri_g < 0.2$ which are sufficiently small in this context – again, one needs to be careful about the exact definition of Ri_g when comparing across different studies, and also it is necessary to remember that this is distinct from keeping the bulk Richardson number Ri (set by the boundary conditions) small. This observation is consistent with previous studies of stably stratified wall-bounded flow simulations (Armenio & Sarkar 2002; García-Villalba & del Álamo 2011; García-Villalba *et al.* 2011*a*) and in homogeneous stratified turbulence (Rohr & Van Atta 1987; Chung & Matheou 2012).

The behaviour of Pr_t becomes more complex at higher values of Ri_g, i.e. for $Ri_g > 0.2$ (Taylor *et al.* 2005; Venayagamoorthy & Stretch 2010; Karimpour & Venayagamoorthy 2014, 2015; Salehipour & Peltier 2015; Wilson & Venayagamoorthy 2015). However, turbulent flows with larger gradient Richardson numbers $Ri_g > 0.2$ do not appear to be accessible in stratified plane Couette flows, for reasons that have been discussed in §5.1. There also exist Re_b-based parameterizations for Pr_t in the literature. Shih *et al.* (2005) and Salehipour & Peltier (2015) reported Pr_t approaching order unity for intermediate to large values of Re_b, which is consistent with our observations. Salehipour & Peltier (2015) also observed larger than $O(1)$ values of Pr_t when the values of Re_b are small, i.e. $O(1)$ to $O(10)$. This is consistent with our outlier group (simulation 12) in figure 7(c) whose Re_b value is $O(10)$ (see figure 7(b)) and the Pr_t value is larger than unity ($Ri_g \gg Ri_f$).

Crucially, all the evidence points towards $Pr_t \sim O(1)$ while the flow is turbulent, with the flow becoming intermittent before Ri_g reaching large values. This is qualitatively different behaviour to that assumed by Ellison (1957), who stated that 'it seems more likely' that turbulence could be 'maintained' at large values of Ri_g with still finite $Ri_f < 1$, and so, from (5.6) and consequences derived from it with further turbulence modelling assumptions, Ellison (1957) was led to the conclusion that Pr_t inevitably reaches large values. Galperin *et al.* (2007) analogously arrived at the conclusion that Pr_t reaches large values in strongly stratified, yet still 'turbulent' flows, in the relatively weak sense that the eddy diffusivities (particularly in the horizontal) remain elevated above molecular values. A potential major point of difference is the central role played in open flows of propagating internal waves, which is not possible in stratified plane Couette flow.

5.4. *Realizability of strongly stratified regime*

Finally, we test the scaling in (B 11) in appendix B, i.e.

$$Fr_h \sim \frac{1}{\sqrt{Ri_g}}, \tag{5.7}$$

for the turbulent Froude number Fr_h. Figure 7(d) shows the DNS results for which an empirical scaling of

$$Fr_h \simeq \frac{0.95}{\sqrt{Ri_g}} \tag{5.8}$$

applies, which is consistent with the Monin–Obukhov prediction in appendix B. The outlier once again corresponds to simulation 12 for which the Re_b value may not be high

enough for the inertially-dominated forward cascade assumption underlying (B 8), i.e. $\varepsilon = U'^3/\ell_h$, to hold.

Given that the maximum Ri_g in fully developed stratified plane Couette flow is approximately 0.2 (see §5.1), the minimum Fr_h that can be obtained in the interior of an stratified plane Couette flow (at large enough Re_b) is approximately 2, following (5.8). However, for the turbulence to reach the strongly stratified regime, it is typically argued that Fr_h needs to be smaller than 0.02 (Brethouwer *et al.* 2007). Therefore, the strongly stratified regime, which is characterised by layering in the density field with characteristic vertical length scale U'/N, may be fundamentally *nonrealizable* in stratified plane Couette flows, at least under the equilibrium conditions we have been considering. Once again, it is important to emphasise that it is the mid-gap gradient Richardson number Ri_g which cannot become large in quasi-steady turbulent stratified plane Couette flow, for any choice of Re and Ri set by the boundary conditions.

5.5. *Summary*

To summarize the results in §5, we have identified certain generic characteristics of the turbulence in the interior regions of stratified plane Couette flows. We find that: the length scale ratio h/L determines the mid-gap Ri_g; Re_b scales linearly with $L^+ \equiv L/\delta_\nu$; Pr_t is of order unity for the range of accessible Ri_g associated with turbulence; and Fr_h is proportional to $Ri_g^{-1/2}$. The scalings, consistent with, and extending the observations of Scotti & White (2016) into the crucially important regime where the externally set bulk $Ri > 0.1$, apply not only to the DNS performed for the present study which cover a wide range of Pr (simulations 1–12), but also to those by DCT as listed in table 1 which covered a wider range of Re (simulations 13–23). These characteristics of stratified plane Couette flows fundamentally relate to the fact that it is the upper and lower walls which impose momentum and heat fluxes on the fluids. These fluxes then dictate the self-similar behaviour of both the mean flow (as characterised by Ri_g) and the turbulence (as characterised by Re_b, Pr_t and Fr_h) in the interior. These results are expected to hold not only for stratified plane Couette flows but also for other constant-flux layers to which the Monin–Obukhov scaling applies. These Monin–Obukhov scalings are intended for regions sufficiently far from the walls. Through the wide range of Prandtl numbers examined, our DNS data suggest that the dynamics away from the walls are Pr-independent for given wall fluxes.

6. Mixing and its parameterization

6.1. *Osborn formulation for stratified plane Couette flow*

Now we turn our attention to the third main theme of interest, namely the parameterization of mixing. Here we use the framework proposed by Osborn (1980) to formulate a parameterization for the turbulent diffusivity $\kappa_t \equiv -\langle\rho' v'\rangle/(d\overline{\rho}/dy) = -B/N^2$. As described in appendix C, key to this formulation is the turbulent flux coefficient, $\Gamma \equiv B/\varepsilon \approx Ri_f/(1 - Ri_f)$. With Γ appropriately parameterized, the Osborn formulation yields an expression for κ_t, i.e.

$$\frac{\kappa_t}{\nu} \approx \frac{Ri_f}{1 - Ri_f}\frac{\varepsilon}{\nu N^2} = \Gamma Re_b. \tag{6.1}$$

It is important to appreciate that key aspects of the Osborn (1980) framework are based on the theoretical considerations of Ellison (1957) and the experimental data of Britter (1974), both associated with stratified flows in the presence of boundary forcing and

thus expected to have at least some similar properties to the turbulence in stratified plane Couette flows. Osborn (1980), following Ellison (1957), postulated that $\Gamma \leqslant 0.2$, or equivalently $Ri_f \leqslant 0.15$, although the inequality in Osborn's original paper has often been ignored subsequently. Interestingly, the experimental data by Britter (1974) (see e.g. pg 8-37 of the thesis) led to his conclusion that 'a critical Richardson flux number (i.e. Ri_f) of approximately 0.2 is predicted'. This is entirely consistent with our results presented in §5 that

$$Ri_f \simeq Ri_g \lesssim 0.2 \tag{6.2}$$

in stratified plane Couette flows for turbulence to be maintained, although as already noted we observe the turbulent Prandtl number remaining of order one, unlike in the model developed by Ellison (1957). Indeed, using this scaling, Γ can be written as a function of the gradient Richardson number Ri_g:

$$\Gamma \approx \frac{Ri_g}{1 - Ri_g}, \tag{6.3}$$

remembering that Ri_g appears to have an upper bound above which turbulence cannot be maintained, even for asymptotically large Re (see figure 18 of DCT), In the literature, however, Γ is often parameterized as a function of Re_b (see e.g. Shih *et al.* (2005)). The connection between the Ri_g-based and Re_b-based scalings for Γ is discussed further in §6.3.1. It follows from (6.1) and (6.3) that

$$\frac{\kappa_t}{\nu} \approx \frac{Ri_g}{1 - Ri_g} Re_b \tag{6.4}$$

in the context of stratified plane Couette flows. Noting that $Pr_t \equiv \nu_t/\kappa_t \approx 1$ in stratified plane Couette flows (as shown in §5) and as also noted by Scotti & White (2016), we can also approximate the turbulent viscosity ν_t with the same scaling for κ_t in (6.4), i.e.

$$\frac{\nu_t}{\nu} \approx \frac{Ri_g}{1 - Ri_g} Re_b. \tag{6.5}$$

6.2. *Numerical results*

These κ_t and ν_t values are estimated directly using their definitions through the flux-gradient relation (A 5) and (5.5) at all locations in the wall-normal direction y that are at least 50 wall units ($y^+ > 50$) away from the walls, where the local equilibrium (A 3) is expected to hold (García-Villalba *et al.* 2011*b*). These results are first plotted in figure 8 to test the Re_b-based parameterizations that are commonly seen in the literature, e.g. those reviewed by Ivey *et al.* (2008) and also discussed in Scotti & White (2016). Our results are plotted in figure 9 to validate the scalings (6.4) and (6.5). Simulation 12, in which the flow is viscously controlled and exhibits spuriously small ($O(1)$ or smaller) or negative (counter-gradient) values of κ_t/ν or ν_t/ν, is not included in the plots to allow the discussion to stay focused on the fully turbulent simulations.

Figure 8 compares the DNS results of κ_t/ν against the classical Re_b-based parameterizations of Osborn (1980) and Shih *et al.* (2005). The DNS data points in figure 8 are sampled *locally* (pointwise) at various y locations across the channel gap interior of stratified plane Couette flows. Within each simulation, the Re_b value stays relatively constant, while the diffusivities span a wider range – the latter is somewhat expected because κ_t and ν_t scale linearly with the mixing lengths ℓ_s^* and ℓ_m^* respectively, both of which increase with the wall distance y_w, as described in §3.1. These Re_b-based scalings are effective in describing the *homogeneous* flow dataset of Shih *et al.* (2005), but they do not provide a good agreement with our DNS data from stratified plane Couette flows

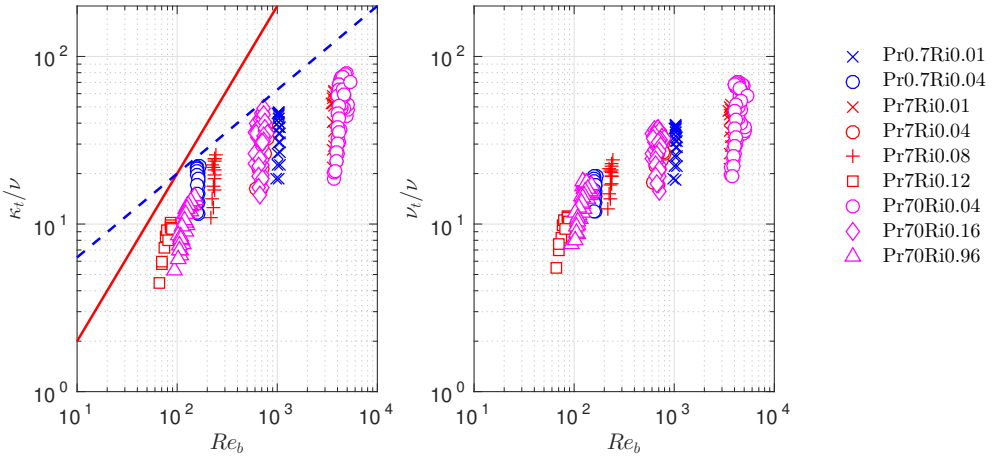

Figure 8: κ_t and ν_t, as defined by (A 5) and (5.5), and both normalised by ν, as a function of Re_b. κ_t, ν_t and Re_b values are computed pointwise in y in the channel gap interior with $y^+ > 50$. Scaling laws of $\kappa_t/\nu = 0.2Re_b$ (Osborn 1980) plotted with a solid line, and $\kappa_t/\nu = 2Re_b^{1/2}$ (Shih *et al.* 2005) plotted with a dashed line, are also shown.

which are inherently *inhomogeneous* due in particular to the presence of the wall. The data for ν_t, which are also plotted in figure 8, behave similarly to κ_t, since the turbulent Prandtl number $Pr_t \equiv \nu_t/\kappa_t$ is approximately unity (as shown in §5.3).

Figure 9 compares the DNS data against the scalings (6.4) and (6.5). The collapse of the DNS data improves significantly when Ri_g is included in the parameterizations, as they capture the critical (linear) dependence of Ri_f on Ri_g. At sufficiently large values of Re_b, i.e. $Re_b \gtrsim 60$, the $\kappa_t/\nu \sim \nu_t/\nu \sim Re_b Ri_g/(1-Ri_g)$ scaling, based on the turbulent kinetic energy budget argument by Osborn (1980) and incorporating Monin–Obukhov scaling for constant-flux layers to account for the importance of the (coupled) value of Ri_g, provides an accurate description of the turbulent diffusivity in stratified plane Couette flows. It is certainly of interest that the Osborn scaling appears to hold, at least qualitatively, even though the underlying assumption of Ellison (1957) (on which the Osborn scaling is at least partially based) that Pr_t becomes large is violated in stratified plane Couette flow. We further discuss this scaling with respect to other previously proposed scalings in the next subsection.

6.3. *Discussions*

6.3.1. Γ *vs.* Re_b

The Shih *et al.* (2005) scalings parameterize the turbulent flux coefficient Γ as a function of the buoyancy Reynolds number Re_b, whereas in the context of stratified plane Couette flow, we propose to parameterize Γ as a function of the gradient Richardson number Ri_g, i.e. $\Gamma \approx Ri_g/(1-Ri_g)$. Here we discuss our results further with respect to the two approaches. Following Shih *et al.* (2005), for $7 < Re_b < 100$, i.e. the 'intermediate' regime, a constant turbulent flux coefficient of $\Gamma = 0.2$, as originally proposed by Osborn (1980) as an upper bound, is used. For $Re_b > 100$, i.e. the 'energetic' regime, Γ was observed by Shih *et al.* (2005) to decrease with Re_b as $\Gamma \propto Re_b^{-1/2}$, although their data only extend to $Re_b \simeq 900$. The scaling for $Re_b > 100$ appears to be consistent with numerical data of mixing layers (Salehipour & Peltier 2015) and field observations (Davis

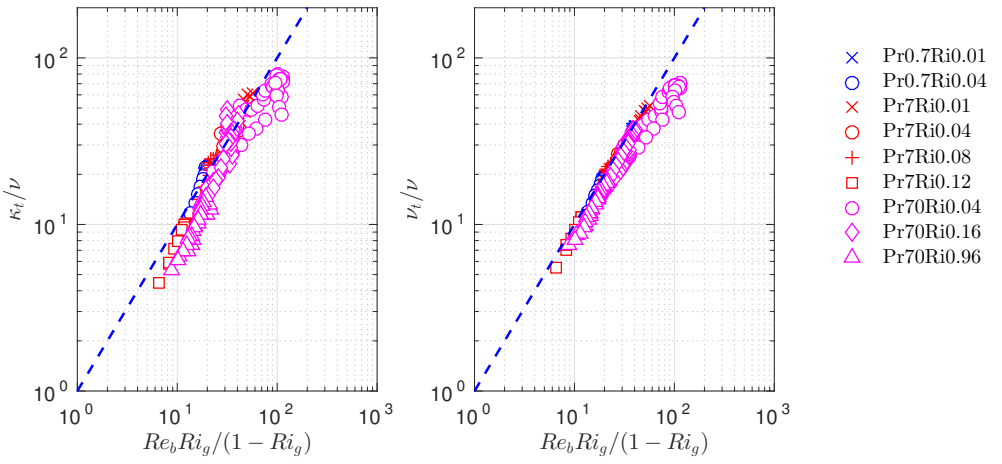

Figure 9: κ_t and ν_t, both normalised by ν, as a function of $Re_b Ri_g/(1-Ri_g)$. κ_t, ν_t, Re_b and Ri_g values are computed pointwise in y in the channel gap interior with $y^+ > 50$. The dashed line marks equality between the abscissa and the ordinate.

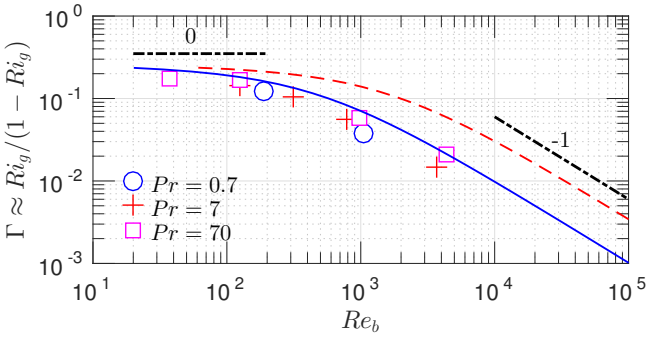

Figure 10: Turbulent flux coefficient Γ (as defined in (C 3)) approximated by $Ri_g/(1-Ri_g)$, where Ri_g is evaluated at mid-gap, plotted as a function of Re_b which is approximated by $k_m L^+$ (as shown in figure 7(b)). Symbols correspond to DNS data. Lines correspond to two different Monin-Obukhov predictions: at $Re = 4250$ (the same Re value as the shown DNS results) plotted with a solid line; and at $Re = 42500$ plotted as a dashed line. Power-law scalings $\Gamma \propto Re_b^n$ with various n values are plotted with dot-dashed lines marked with the values of n.

& Monismith 2011; Walter *et al.* 2014). One shortcoming of this scaling is, however, that the value of $\kappa_t/\nu = \Gamma Re_b \propto Re_b^{1/2}$ becomes infinite when one considers the mixing of a passive scalar, since $Re_b \to \infty$ as $N^2 \to 0$ and ε and ν remain finite. In contrast, experiments by Holford & Linden (1999) suggested that the eddy diffusivity approaches a finite value in the zero-stratification limit. Moreover, Chung & Matheou (2012) also reported saturation of eddy diffusivity for large-to-infinite values of Re_b and offered a phenomenological explanation from the perspective of competing length scales.

The scalings (6.4) and (6.5), by including the Ri_g-dependence, circumvent this problem at the zero-stratification limit where $Re_b \to \infty$ as $Ri \to 0$, as $\Gamma \propto Re_b^{-1}$ in the limit of $Re_b \to \infty$ (as shown in figure 10). These scalings also provide a convenient framework to interpret the change of power-law exponent in Re_b in the scaling of Γ (Barry *et al.*

2001; Shih *et al.* 2005). This is demonstrated in figure 10, where the characteristic values of turbulent flux coefficient Γ in the interior of stratified plane Couette flow, as approximated by $Ri_g/(1 - Ri_g)$, are plotted against the corresponding Re_b values. The Monin–Obukhov predictions from the model presented in §3 are also shown in figure 10 for two values of bulk Reynolds number Re, i.e. $Re = 4250$ and $Re = 42500$.

As shown in figure 10, when Re_b is smaller than $O(100)$, which corresponds to the $h/L > 1$ regime in terms of the characteristic Ri_g value (see figure 7(a)), Ri_g remains a constant value of approximately 0.2 at mid-gap as given in (5.2). The characteristic turbulent flux coefficient $\Gamma \approx Ri_g/(1 - Ri_g) \approx 0.25$ is thus a constant. This regime is reminiscent of Shih *et al.* (2005)'s 'intermediate' regime where Γ is a constant of 0.2 independent of Re_b, the upper bound as argued by Osborn (1980). Consequently, $\kappa_t/\nu = \Gamma Re_b \propto Re_b$ in this regime. This regime may be thought of as a saturated regime for Γ, as Ri_g is close to its maximum value for sustained turbulence, consistent with the underlying assumptions of Osborn (1980).

When Re_b is large, e.g. $Re_b > O(1000)$ for $Re = 4250$, which corresponds to the $h/L \ll 1$ limit in terms of Ri_g (figure 7(a)), the characteristic Ri_g can be estimated via (B 3) by taking the limit of $h/L \to 0$ or $L^+ \to \infty$, which yields

$$Ri_g = \frac{k_m}{k_s}\frac{h}{L} = \frac{k_m}{k_s}\frac{Re_{\tau,\infty}}{L^+} \approx \frac{k_m^2}{k_s}\frac{Re_{\tau,\infty}}{Re_b}, \tag{6.6}$$

where $Re_{\tau,\infty}$ denotes the friction Reynolds number for the case of passive scalar ($L^+ \to \infty, Re_b \to \infty$). With $Ri_g \ll 1$ in this limit, $\Gamma \approx Ri_g/(1 - Ri_g) \approx Ri_g$. Following (6.6), the turbulent flux coefficient $\Gamma \approx Ri_g \propto Re_b^{-1}$ holds for large Re_b in the limit of zero Richardson number. It is important to appreciate that this is not in itself inconsistent with Osborn (1980)'s argument, as 0.2 is the upper bound he proposes for Γ. It follows from (6.6) that, in the limit of $Re_b \to \infty$, $\kappa_t/\nu = \Gamma Re_b = k_m^2 k_s^{-1} Re_{\tau,\infty}$ approaches a constant which depends solely on $Re_{\tau,\infty}$ (which itself is a function of the bulk Reynolds number Re). This regime corresponds to the scenario of mixing a nearly passive scalar, a regime that finds no counterpart in the regimes presented in Shih *et al.* (2005). As is apparent in figure 10, this regime only really becomes clearly identifiable for $Re_b \gtrsim 1000$, larger values than those presented in Shih *et al.* (2005).

There exists a transitional regime where Γ decays monotonically with Re_b, but with a slower rate than the $\Gamma \propto Re_b^{-1}$ power law in the weakly stratified limit. This transitional regime at least superficially resembles Shih *et al.* (2005)'s 'energetic' regime where $\Gamma \propto Re_b^{-1/2}$ and $\kappa_t/\nu \propto Re_b^{1/2}$ in the sense that Γ starts to decrease with Re_b. Of course it is important to remember that this resemblance may be entirely fortuitous, due not least to the necessity of connecting two different asymptotic regimes, and the marked difference of the two flow geometries and forcing mechanisms of the turbulence. The critical Re_b, which marks the transition from the small-Re_b regime to this intermediate-Re_b regime, appears to be approximately 100 for $Re = 4250$. However, as shown by Monin–Obukhov predictions plotted in figure 10 for $Re = 42500$, the exact value of the critical Re_b is not unique but rather moves to larger values for larger Re, and also the specific numerical values are dependent on the averaging volumes for ε and N in spatially inhomogeneous flows.

To summarize, in the small-Re_b regime with $Re_b \lesssim 100$, Γ and Ri_g are independent of Re_b, and in the weakly stratified $Re_b \gtrsim 1000$ regime with small Ri, $\Gamma \approx Ri_g \propto Re_b^{-1}$ where the mixing resembles that of a nearly passive scalar. It is within the transitional regime between these two where Ri_g, and thus also $\Gamma \approx Ri_g/(1 - Ri_g)$, both become dependent on Re_b. The coupling between Ri_g and Re_b, as is dictated by Monin–Obukhov

scalings in stratified plane Couette flow, may offer some explanation for the commonly observed variations of Γ with respect to Re_b (as presented, for example, in Shih *et al.* (2005)). It is very important to stress that this picture emerges from wall-bounded stratified shear flows, consistent with the arguments and data underpinning the model of Osborn (1980). In particular, the picture depends strongly on the observation in stratified plane Couette flow that $Ri_f \simeq Ri_g$ and that $Ri_g \lesssim 0.2$ for sustained turbulence.

6.3.2. Γ *vs.* Fr_h

A recent study by Maffioli *et al.* (2016) utilised the parameter Fr_h to scale turbulent flux coefficient Γ in triply periodic body-forced turbulence. Critically its forcing is very different from the forcing which we consider. In stratified plane Couette flow, the forcing at the boundary has to penetrate into the interior to drive turbulent mixing, while the forcing in the flow considered by Maffioli *et al.* (2016) is introduced throughout the interior of the flow, and so there is no dynamical 'barrier' to the energy being available to stratified turbulent mixing throughout the flow. For the $Fr_h > 1$ regime, which corresponds to our small-Ri_g weakly stratified regime, they proposed that $\Gamma \propto Fr_h^{-2}$. A similar dependence of Γ on the bulk Froude number $Fr_0 = U/\sqrt{G'H\cos\theta}$ (defined using characeristic scales for the current velocity U along a slope of angle θ to the horizontal, depth H and reduced gravity $G'\cos\theta$) i.e. $\Gamma \propto Fr_0^{-2}$, has also been reported for relatively weakly stratified density currents when $Fr_0 \gg 1$ (Wells *et al.* 2010). It has been shown that $Fr_h \propto Ri_g^{-1/2}$ holds in stratified plane Couette flows (see §5.4), and therefore the $\Gamma \propto Fr_h^{-2}$ scaling for Γ is consistent with our approximation $\Gamma \approx Ri_g/(1 - Ri_g) \approx Ri_g$ (for small Ri_g). For the small-Fr_h regime, Maffioli *et al.* (2016) reported a Γ value approaching a constant 0.33 at Fr_h values of $O(10^{-2})$ which are accessible in their forced simulations. In stratified plane Couette flows, where the minimum Fr_h is of $O(1)$ as shown in figure 7(d), our results suggest a fixed value of $0.2/(1 - 0.2) = 0.25$ that is closer to the upper bound of the Osborn (1980) formulation, i.e. $\Gamma = 0.2$, which is also the value reported by Wells *et al.* (2010) in their intermediate $Fr_0 \sim 1$ regime.

6.3.3. *Non-monotonic mixing?*

Pioneering work on turbulent mixing in stratified flows (Linden 1979, 1980; Fernando 1991; Park *et al.* 1994; Holford & Linden 1999) revealed the possibility of non-monotonic behaviour in the stratified mixing, i.e. the buoyancy flux does not necessarily increase monotonically but rather can plateau and then decrease with increasing stratification. Non-monotonic mixing was proposed to be the mechanism for the formation of generic features in stratified fluids such as relatively well-mixed and deep 'layers' separated by relatively shallow and sharp 'interfaces', as originally proposed by Phillips (1972). Such non-monotonic mixing has also been observed in time-dependent stratified shear layers (Caulfield & Peltier 2000; Smyth *et al.* 2001; Mashayek *et al.* 2013; Salehipour & Peltier 2015). Potentially associated spontaneous layer formation has been observed in stratified Taylor-Couette flows in the annular region between two concentric cylinders (Oglethorpe *et al.* 2013) and in flows where the mixing is induced by translating rods (Park *et al.* 1994; Holford & Linden 1999).

In fully developed turbulent stratified plane Couette flow, however, such non-monotonic mixing is not observed. The turbulent flux coefficient $\Gamma \equiv B/\varepsilon$, which measures the buoyancy flux in dimensionless form, increases monotonically with Ri_g, a dimensionless measure of the stratification. We hypothesize that this behaviour is due to the range of Ri_g which is accessible in turbulent stratified plane Couette flows where the maximum gradient Richardson number is approximately 0.2 (as discussed in §5.1). Effectively, it appears that stratified plane Couette flows can only access the weakly stratified 'left flank'

of the non-monotonic mixing curve with stratification postulated by Phillips (1972) and observed widely in experiments (see, for example, the classic review of Linden (1979)).

6.3.4. *Effect of Prandtl number*

Throughout our discussion in this section, there is no explicit dependence of the normalised values of κ_t/ν (or ν_t/ν) on the molecular Prandtl number Pr. This is probably due to the fact that the Re_b values examined here are sufficiently large, i.e. $Re_b \gtrsim 60$ (see figure 8), so that the molecular properties of the fluid have no effect on the turbulent mixing in the channel gap interior. Variation in Prandtl number Pr may indeed be important for a small-Re_b 'molecular' regime with $Re_b \sim O(1-10)$ (Shih *et al.* 2005; Ivey *et al.* 2008; Bouffard & Boegman 2013) which is not the focus of the present study. Motivated by experimental results, Barry *et al.* (2001) included Pr in their parameterizations of κ_t even at large values of Re_b up to $O(10^4 - 10^5)$. This discrepancy, similarly to the situation with respect to Maffioli *et al.* (2016), is most likely associated with the differences in turbulence forcing mechanisms, i.e. shear driven by the walls as in the present study, versus grid stirring as in Barry *et al.* (2001) .

7. Concluding remarks

In this paper, we have investigated stratified turbulence in fully developed stratified plane Couette flows, through DNS at a wide range of Pr. We use Monin–Obukhov similarity theory as a guide to interpret the numerical results. In particular, we have highlighted the relevance of heat and momentum fluxes to the turbulence characteristics in the channel gap interior, as well as the implications of these similarity scalings for diapycnal mixing.

The dynamical role of Prandtl number appears to be subtle in stratified plane Couette flows. On one hand, the near-wall temperature structure (see in figure 5) is strongly Pr-dependent (as discussed in §3). Therefore, Pr has an explicit effect on the heat flux q_w through the wall (as shown in §4). This quantity is relevant for the Monin–Obukhov scalings of the interior turbulence as presented in §5. On the other hand, there is no direct impact of Pr on the interior turbulence whose self-similar characteristics are determined solely by the wall fluxes (u_τ^2 and q_w) and the buoyancy parameter ($g\alpha_V$), which is in agreement with Monin–Obukhov similarity theory and the DNS results covering a wide range of Pr.

Monin–Obukhov similarity theory has motivated several useful scalings which are found to be consistent with DNS results, as shown in §5. The roles of the length scales h, L and δ_ν are highlighted through their connections to flow diagnostics such as Ri_g (which is determined by h/L) and Re_b (which is determined by L/δ_ν). It is somewhat surprising to discover an upper limit for Ri_g (or equivalently, a lower limit of $Fr_h \propto Ri_g^{-1/2}$) in stratified plane Couette flow, irrespective of the externally set boundary conditions, where the turbulence is influenced strongly by the wall fluxes. This suggests that the 'strongly stratified regime' in the sense described in Brethouwer *et al.* (2007) might not be realizable in this type of flows, at least under equilibrium conditions. This observation motivates the further question as to how this strongly stratified regime can be accessed 'naturally', i.e. without specific forcing or initial conditions.

Within the range of Ri_g accessible in stratified plane Couette flows, i.e. $Ri_g \lesssim 0.2$, the $\kappa_t/\nu \sim Re_b Ri_g/(1-Ri_g)$ scaling holds for the diapycnal diffusivity as shown in §6. This reinforces the now commonly held belief that Re_b is not the only relevant parameter in describing diapycnal mixing, and in particular, we have further highlighted the role of Ri_g which has also been addressed by recent studies by Salehipour & Peltier (2015) and

Maffioli *et al.* (2016) (although Maffioli *et al.* (2016) used Fr_h as the parameter instead, Fr_h may be related to Ri_g). As noted by Lozovatsky & Fernando (2013) and discussed in detail in this paper in §6.3, Re_b and Ri_g may or may not be independent parameters depending on the parameter range and flow geometry. Indeed, in statistically stationary turbulent stratified plane Couette flow, we find that the characteristic mid-gap value of Ri_g is set by the prevailing properties of the turbulent flow, and is not an external parameter independently adjustable from the turbulence. This property is instrumental in explaining the variation of the turbulent flux coefficient $\Gamma \approx Ri_g/(1 - Ri_g)$. No non-monotonic mixing behaviour is observed, which we hypothesize to be due to the range of Ri_g accessible in such constant-flux layers. Moreover, our results strongly indicate that the Prandtl number Pr does not have an effect on turbulent mixing away from the walls, at least for the intermediate to large Re_b values examined, i.e. $Re_b \gtrsim 60$, as shown in figure 8.

In the present study, we have investigated fully developed stratified plane Couette flows for which the turbulent kinetic energy balance is, to a good approximation, in a simple local equilibrium (A 3) that involves shear production, viscous dissipation and diapycnal mixing, consistently with the classical modelling assumptions of Osborn (1980) – mixing is thus not particularly 'efficient' with $\Gamma \leqslant 0.25$. Possible nonlocal and nonstationary behaviour in stratified plane Couette flows is of great interest, particularly with regard to its mixing properties, and is the topic of ongoing investigations. Finally, it is important to remember that the analysis in this paper has focused on doubly-bounded constant-flux layers with momentum and buoyancy fluxes injected through smooth boundaries. Flows in geophysical settings can be considerably more complex due to surface roughness or imposed pressure gradient, (mentioning just two examples) and such additional complexities are not captured by this investigation of stratified plane Couette flows. For example, the turbulent diffusivities may exhibit strong anisotropy in horizontal and vertical directions which needs to be treated by more sophisticated models (e.g. Sukoriansky & Galperin 2013; Tastula *et al.* 2015) than the canonical Monin–Obukhov theory.

We thank four anonymous referees whose constructive comments have helped improve the paper. The EPSRC Programme Grant EP/K034529/1 entitled 'Mathematical Underpinnings of Stratified Turbulence' is gratefully acknowledged for supporting the research presented here. We would like to thank Dr E. Deusebio for sharing the Deusebio *et al.* (2015) data and helpful discussions on this topic. Dr M. van Reeuwijk is gratefully acknowledged for suggesting an error in an early version of the manuscript.

Appendix A. Monin–Obukhov scaling: dimensional quantities

A.1. *Mean shear and temperature gradient*

Monin–Obukhov similarity theory (see e.g. Wyngaard (2010)) suggests that the friction velocity u_τ, the wall heat flux q_w and the buoyancy parameter $g\alpha_V$ are the only relevant dimensional quantities for the dynamics of the turbulence sufficiently far away from the walls. These quantities form the similarity length scale L as defined in (1.1). According to Monin–Obukhov theory, the mean shear S and temperature gradient $d\Theta/dy$ vary self-similarly with respect to the transformed wall-normal coordinate $\xi \equiv y_w/L$, i.e. the wall-normal distance y_w normalised by L. These formulae for S and $d\Theta/dy$ are shown in

(3.11), and they can be rewritten, for simplicity, as

$$S \equiv \frac{\partial U}{\partial y} = \frac{u_\tau}{\ell_m^*} \qquad \text{and} \qquad \frac{\partial \Theta}{\partial y} = \frac{\theta_\tau}{\ell_s^*} = \frac{q_w/u_\tau}{\ell_s^*}, \tag{A 1}$$

where ℓ_m^* and ℓ_s^* are the mixing lengths for momentum and scalar respectively. The lengths ℓ_m^* and ℓ_s^* are both functions of y_w (or $\xi \equiv y_w/L$), and their closed-form expressions for the channel gap interior, following Monin–Obukhov theory, are shown in (3.13). With (A 1) and (1.1), the squared buoyancy frequency can be written as

$$N^2 \equiv g\alpha_V \frac{\partial \Theta}{\partial y} = g\alpha_V \frac{q_w/u_\tau}{\ell_s^*} = \frac{u_\tau^2}{k_m L \ell_s^*}. \tag{A 2}$$

A.2. *Turbulent kinetic energy budget*

Far enough away from the walls, i.e. $y^+ \equiv y_w/\delta_\nu > 50$, in fully developed turbulent stratified plane Couette flows, the balance of the turbulent kinetic energy involves shear production P, dissipation ε and buoyancy flux $B \equiv -\langle \rho' v' \rangle/(g\rho_0)$ as the dominant terms (García-Villalba *et al.* 2011*b*), i.e.

$$P \approx \varepsilon - B, \tag{A 3}$$

where the shear production scales as

$$P \equiv \langle u'v' \rangle S \sim u_\tau^2 S \sim \frac{u_\tau^3}{\ell_m^*}. \tag{A 4}$$

Invoking the definition of turbulent diffusivity κ_t via the flux-gradient relation, i.e.

$$\kappa_t \equiv -\frac{\langle \rho' v' \rangle}{d\overline{\rho}/dy}, \tag{A 5}$$

the buoyancy flux B can be written as $B = -\kappa_t N^2$. Following the mixing length specifications (3.6) and (3.10), as well as the expression for N^2 in (A 2), B can be rewritten as

$$B = -\ell_s^* u_\tau N^2 = -\frac{u_\tau^3}{k_m L}. \tag{A 6}$$

As is shown in §5, in figure 7 in particular, the flux Richardson number, defined as $Ri_f \equiv -B/P$, is typically smaller than 0.2 in stratified plane Couette flows. One may make the further approximation $-B \ll P$ in (A 3), which results in the following scaling for ε:

$$\varepsilon \approx (1 - Ri_f)P \sim P \sim \frac{u_\tau^3}{\ell_m^*}. \tag{A 7}$$

Appendix B. Monin–Obukhov scaling: dimensionless quantities

The gradient Richardson number Ri_g can be evaluated from (A 1) and (A 2):

$$Ri_g \equiv \frac{N^2}{S^2} = \frac{u_\tau^2}{k_m L \ell_s^*} \frac{\ell_m^{*2}}{u_\tau^2} = \frac{\ell_m^{*2}}{k_m L \ell_s^*}. \tag{B 1}$$

With ℓ_m^* and ℓ_s^* prescribed by Monin–Obukhov theory shown in (3.13), Ri_g can be written as a function of the transformed wall-normal coordinate ξ, i.e.

$$Ri_g(\xi) = \frac{k_m}{k_s} \frac{\xi^{-1} + \beta_s}{(\xi^{-1} + \beta_m)^2}, \tag{B 2}$$

where k_m, k_s, β_m and β_s are all dimensionless constants in Monin–Obukhov theory (§3.1).

We are particularly interested in the Ri_g value at $y = 0$ ($y_w = h$ or $\xi = h/L$), a location characteristic of the mid-gap plateau as shown in figure 5. Such a characteristic Ri_g value can be obtained by evaluating (B 2) at $\xi = h/L$:

$$Ri_g|_{y=0} = \frac{k_m}{k_s}\frac{(h/L)^{-1} + \beta_s}{[(h/L)^{-1} + \beta_m]^2}, \tag{B 3}$$

an expression that has no explicit dependence on the Prandtl number Pr. The influence of Pr on the interior Ri_g is indirect through the modulation of wall fluxes which determine the Obukhov length scale L as defined in (1.1).

Combining (A 2) and (A 7), one can obtain an estimate for the buoyancy Reynolds number Re_b:

$$Re_b \equiv \frac{\varepsilon}{\nu N^2} \sim \frac{u_\tau L}{\nu}\frac{\ell_s^*}{\ell_m^*}k_m = L^+\frac{\ell_s^*}{\ell_m^*}k_m. \tag{B 4}$$

As discussed in §3.1, the ratio ℓ_s^*/ℓ_m^* is typically of order unity, as prescribed by Monin–Obukhov theory. The above scaling (cf. Scotti & White (2016)) thus becomes

$$Re_b \sim L^+ k_m. \tag{B 5}$$

Following (A 4) and (A 6), the flux Richardson number Ri_f can be estimated as

$$Ri_f \equiv \frac{-B}{P} \sim \frac{\ell_m^*}{k_m L}. \tag{B 6}$$

With (B 1), the above scaling becomes $Ri_f \sim (\ell_s^*/\ell_m^*)Ri_g$. Again, with ℓ_s^*/ℓ_m^* being $O(1)$, one obtains

$$Ri_f \sim Ri_g, \tag{B 7}$$

which is consistent with the observations of DCT (see e.g. their figure 13).

The other relevant parameter is the horizontal turbulent Froude number $Fr_h \equiv U'/(\ell_h N)$ (e.g. Billant & Chomaz (2001); Brethouwer *et al.* (2007)) which can be estimated by assuming

$$\varepsilon = \frac{U'^3}{\ell_h} \tag{B 8}$$

for the horizontal motions of the integral scale ℓ_h undergoing a forward cascade. Fr_h can then be estimated as (see e.g. Maffioli *et al.* (2016))

$$Fr_h \equiv \frac{U'}{\ell_h N} \sim \frac{\varepsilon}{NU'^2} \sim \frac{\varepsilon}{Nu_\tau^2}, \tag{B 9}$$

for stratified plane Couette flows. Upon substituting (A 2) and (A 7) into (B 9), we obtain

$$Fr_h^2 \sim \frac{\varepsilon^2}{N^2 u_\tau^4} \sim \frac{u_\tau^6}{\ell_m^{*2}\frac{u_\tau^2}{k_m L \ell_s^*}u_\tau^4} = \frac{k_m L \ell_s^*}{\ell_m^{*2}}. \tag{B 10}$$

Using (B 1), one obtains a scaling for Fr_h as a function of Ri_g:

$$Fr_h \sim \frac{1}{\sqrt{Ri_g}}. \tag{B 11}$$

Appendix C. Osborn formulation for the turbulent flux coefficient

The steady-state turbulent kinetic energy balance $P \approx \varepsilon - B$ leads to

$$-B \approx \frac{Ri_f}{1 - Ri_f}\varepsilon. \tag{C 1}$$

Dividing the above equation by νN^2 and using $B = -\kappa_t N^2$,

$$\frac{\kappa_t}{\nu} \approx \frac{Ri_f}{1 - Ri_f}\frac{\varepsilon}{\nu N^2} = \Gamma Re_b, \tag{C 2}$$

where

$$\Gamma \equiv \frac{B}{\varepsilon} \approx \frac{Ri_f}{1 - Ri_f} \tag{C 3}$$

is the turbulent flux coefficient, and it is a fundamental question how Γ (commonly referred to as 'mixing efficiency' in the oceanographic literature) is to be parameterized (see e.g. Ivey *et al.* (2008)).

REFERENCES

Armenio, V. & Sarkar, S. 2002 An investigation of stably stratified turbulent channel flow using large-eddy simulation. *J. Fluid Mech.* **459**, 1–42.

Barry, M. E., Ivey, G. N., Winters, K. B. & Imberger, J. 2001 Measurements of diapycnal diffusivities in stratified fluids. *J. Fluid Mech.* **442**, 267–291.

Batchelor, G.K. 1959 Small-scale variation of convected quantities like temperature in turbulent fluid. Part 1. General discussion and the case of small conductivity. *J. Fluid Mech.* **5**, 113–133.

Bewley, T. R. 2010 *Numerical Renaissance: Simulation, Optimization, and Control*. Renaissance, San Diego, California (available at http://numerical-renaissance.com).

Billant, P. & Chomaz, J.-M. 2001 Self-similarity of strongly stratified inviscid flows. *Phys. Fluids* **13**, 1645–1651.

Bouffard, D. & Boegman, L. 2013 A diapycnal diffusivity model for stratified environmental flows. *Dyn. Atmos. Oceans* **61-62**, 14–34.

Bradshaw, P. & Huang, G. P. 1995 The law of the wall in turbulent flow. *Proc. R. Soc. Lond. A* **451**, 165–188.

Brethouwer, G., Billant, P., Lindborg, E. & Chomaz, J.-M. 2007 Scaling analysis and simulation of strongly stratified turbulent flows. *J. Fluid Mech.* **585**, 343–368.

Britter, R.E. 1974 An experiment on turbulence in a density stratified fluid. PhD thesis, Monash University, Victoria, Australia.

de Bruyn Kops, S. M. 2015 Classical scaling and intermittency in strongly stratified boussinesq turbulence. *J. Fluid Mech.* **775**, 436–463.

Caulfield, C. P. & Peltier, W. R. 2000 The anatomy of the mixing transition in homogeneous and stratified free shear layers. *J. Fluid Mech.* **413**, 1–47.

Caulfield, C. P., Tang, W. & Plasting, S. C. 2004 Reynolds number dependence of an upper bound for the long-time-averaged buoyancy flux in plane stratified couette flow. *J. Fluid Mech.* **498**, 315–332.

Chung, D. & Matheou, G. 2012 Direct numerical simulation of stationary homogeneous stratified sheared turbulence. *J. Fluid Mech.* **696**, 434–467.

Davidson, P. A. 2004 *Turbulence: An Introduction for Scientists and Engineers*. Oxford University Press.

Davis, K. A. & Monismith, S. G. 2011 The modification of bottom boundary layer turbulence and mixing by internal waves shoaling on a barrier reef. *J. Phys. Oceanogr.* **41**, 2223–2241.

Deusebio, E., Caulfield, C. P. & Taylor, J. R. 2015 The intermittency boundary in stratified plane Couette flow. *J. Fluid Mech.* **781**, 298–329, referred to in the text as DCT.

Diamessis, P. J., Spedding, G. R. & Domaradzki, J. A. 2011 Similarity scaling and vorticity

structure in high-Reynolds-number stably stratified turbulent wakes. *J. Fluid Mech.* **671**, 52–95.

van Driest, E. R. 1956 On turbulent flow near a wall. *J. Aeronaut. Sci.* **23**, 1007–1011.

Eaves, T. S. & Caulfield, C. P. 2015 Disruption of SSP/VWI states by a stable stratification. *J. Fluid Mech.* **784**, 548–564.

Ellison, T.H. 1957 Turbulent transport of heat and momentum from an infinite rough plane. *J. Fluid Mech.* **2**, 456–466.

Fernando, H. J. S. 1991 Turbulent mixing in stratified fluids. *Annu. Rev. Fluid Mech.* **23**, 455–493.

Flores, O. & Riley, J. J. 2011 Analysis of turbulence collapse in stably stratified surface layers using direct numerical simulation. *Bound.-Lay. Meteorol.* **139**, 241–259.

Foken, T. 2006 50 years of the Monin–Obukhov similarity theory. *Bound.-Lay. Meteorol.* **119**, 431–447.

Galperin, B., Sukoriansky, S. & Anderson, P. S. 2007 On the critical richardson number in stably stratified turbulence. *Atmos. Sci. Let.* **8**, 65–69.

García-Villalba, M. & del Álamo, J. C. 2011 Turbulence modification by stable stratification in channel flow. *Phys. Fluids* **23**, 045104.

García-Villalba, M., Azagra, E. & Uhlmann, M. 2011*a* A numerical study of turbulent stably-stratified plane Couette flow. In *High Performance Computing in Science and Engineering '10* (ed. W. E. Nagel *et al.*), pp. 251–261. Springer-Verlag.

García-Villalba, M., Azagra, E. & Uhlmann, M. 2011*b* Mixing efficiency in stably-stratified plane Couette flow. In *Proceedings of the 7th Int. Symp. on Stratified Flows, Rome, Italy*.

Holford, J. M. & Linden, P. F. 1999 Turbulent mixing in a stratified fluid. *Dynam. Atmos. Oceans* **30**, 173–198.

Howard, L. N. 1961 Note on a paper of John W. Miles. *J. Fluid Mech.* **10**, 509–512.

Ivey, G. N., Winters, K. B. & Koseff, J. R. 2008 Density stratification, turbulence, but how much mixing? *Annu. Rev. Fluid Mech.* **40**, 169.

Karimpour, F. & Venayagamoorthy, S. K. 2014 A simple turbulence model for stably stratified wall-bounded flows. *J. Geophys. Res.* **119**, 870–880.

Karimpour, F. & Venayagamoorthy, S. K. 2015 On turbulent mixing in stably stratified wall-bounded flows. *Phys. Fluids* **27**, 046603.

Lilly, D. K. 1983 Stratified turbulence and the mesoscale variability of the atmosphere. *J. Atoms. Sci.* **40**, 749–761.

Linden, P. F. 1979 Mixing in stratified fluids. *Geophys. Astro. Fluid Dyn.* **13**, 3–23.

Linden, P. F. 1980 Mixing across a density interface produced by grid turbulence. *J. Fluid Mech.* **100**, 691–703.

Lozovatsky, I. D. & Fernando, H. J. S. 2013 Mixing efficiency in natural flows. *Phil. Trans. R. Soc. A* **371**, 20120213.

Maffioli, A., Brethouwer, G. & Lindborg, E. 2016 Mixing efficiency in stratified turbulence. *J. Fluid Mech.* **794**, R3.

Maffioli, A. & Davidson, P. A. 2015 Dynamics of stratified turbulence decaying from a high buoyancy reynolds number. *J. Fluid Mech.* **786**, 210–233.

Mahrt, L. 1999 Stratified atmospheric boundary layers. *Bound.-Lay. Meteorol.* **90**, 375–396.

Mahrt, L. 2014 Stably stratified atmospheric boundary layers. *Annu. Rev. Fluid Mech.* **46**, 23–45.

Mashayek, A., Caulfield, C. P. & Peltier, W. R. 2013 Time-dependent, non-monotonic mixing in stratified turbulent shear flows: Implications for oceanographic estimates of buoyancy flux. *J. Fluid Mech.* **736**, 570–593.

Mater, B. D. & Venayagamoorthy, S. K. 2014 The quest for an unambiguous parameterization of mixing efficiency in stably stratified geophysical flows. *Geophys. Res. Lett.* **41**, 4646–4653.

Miles, J. W. 1961 On the stability of heterogeneous shear flows. *J. Fluid Mech.* **10**, 496–508.

Oglethorpe, R. L. F., Caulfield, C. P. & Woods, A. W. 2013 Spontaneous layering in stratified turbulent Taylor–Couette flow. *J. Fluid Mech.* **721**, R3.

1054 Osborn, T. R. 1980 Estimates of the local rate of vertical diffusion from dissipation
1055 measurements. *J. Phys. Oceanogr.* **10**, 83–89.

1056 Park, Y. G., Whitehead, J. A. & Gnanadeskian, A. 1994 Turbulent mixing in stratified
1057 fluids: layer formation and energetics. *J. Fluid Mech.* **279**, 279–311.

1058 Peltier, W. R. & Caulfield, C. P. 2003 Mixing efficiency in stratified shear flows. *Annu.*
1059 *Rev. Fluid Mech.* **35**, 135–167.

1060 Pham, H. T., Sarkar, S. & Winters, K. B. 2013 Large-eddy simulation of deep-cycle
1061 turbulence in an Equatorial Undercurrent model. *J. Phys. Oceanogr.* **43**, 2490–2502.

1062 Phillips, O. M. 1972 Turbulence in a strongly stratified fluid – is it unstable? *Deep-Sea Res.*
1063 **19**, 79–81.

1064 Pope, S. B. 2000 *Turbulent Flows*. Cambridge University Press.

1065 van Reeuwijk, M. & Hadžiabdić, M. 2015 Modelling high schmidt number turbulent mass
1066 transfer. *Int. J. Heat Fluid Fl.* **51**, 42–49.

1067 Riley, J. J. & de Bruyn Kops, S. M. 2003 Dynamics of turbulence strongly influenced by
1068 buoyancy. *Phys. Fluids* **15**, 2047.

1069 Riley, J. J. & Lindborg, E. 2012 Recent progress in stratified turbulence. In *Ten Chapters in*
1070 *Turbulence* (ed. P. A. Davidson, Y. Kaneda & K. R. Sreenivasan), pp. 269–317. Cambridge
1071 University Press.

1072 Rohr, J. & Van Atta, C. 1987 Mixing efficiency in stably stratified growing turbulence. *J.*
1073 *Geophys. Res.* **92**, 5481–5488.

1074 Salehipour, H., Caulfield, C. P. & Peltier, W.R. 2016 Turbulent mixing due to the
1075 Holmboe wave instability at high Reynolds number. *J. Fluid Mech.* **803**, 591–621.

1076 Salehipour, H., Peltier, W.R. & Mashayek, A. 2015 Turbulent diapycnal mixing in
1077 stratified shear flows: the influence of Prandtl number on mixing efficiency and transition
1078 at high Reynolds number. *J. Fluid Mech.* **773**, 178–223.

1079 Salehipour, H. & Peltier, W. R. 2015 Diapycnal diffusivity, turbulent Prandtl number and
1080 mixing efficiency in Boussinesq stratified turbulence. *J. Fluid Mech.* **775**, 464–500.

1081 Schlichting, H. & Gersten, K. 2003 *Boundary-Layer Theory*. Springer.

1082 Scotti, A. 2015 Biases in Thorpe-scale estimates of turbulence dissipation. Part II: Energetics
1083 arguments and turbulence simulations. *J. Geophys. Res.* **45**, 2522–2543.

1084 Scotti, A. & White, B. 2016 The mixing efficiency of stratified turbulent boundary layers. *J.*
1085 *Phys. Oceanogr.* **46**, 3181–3191.

1086 Shih, L. H., Koseff, J. R., Ferziger, J. H. & Rehmann, C. R 2000 Scaling and
1087 parameterization of stratified homogeneous turbulent shear flow. *J. Fluid Mech.* **412**,
1088 1–20.

1089 Shih, L. H., Koseff, J. R., Ivey, G. N. & Ferziger, J. H. 2005 Parameterization of turbulent
1090 fluxes and scales using homogeneous sheared stably stratified turbulence simulations. *J.*
1091 *Fluid Mech.* **525**, 193–214.

1092 Smyth, W. D. & Moum, J. N. 2013 Marginal instability and deep cycle turbulence in the
1093 eastern equatorial Pacific Ocean. *Geophys. Res. Lett.* **40**, 6181–6185.

1094 Smyth, W. D., Moum, J. N. & Caldwell, D. R. 2001 The efficiency of mixing in turbulent
1095 patches: Inferences from direct simulations and microstructure observations. *J. Phys.*
1096 *Oceanogr.* **31**, 1969–1992.

1097 Sukoriansky, S. & Galperin, B. 2013 An analytical theory of the buoyancy–Kolmogorov
1098 subrange transition in turbulent flows with stable stratification. *Phil. Trans. R. Soc. A*
1099 **371**, 20120212.

1100 Tang, W., Caulfield, C. P. & Kerswell, R. R. 2009 A prediction for the optimal
1101 stratification for turbulent mixing. *J. Fluid Mech.* **634**, 487–497.

1102 Tastula, E.-M., Galperin, B., Sukoriansky, S., Luhar, A. & Anderson, P. 2015 The
1103 importance of surface layer parameterization in modeling of stable atmospheric boundary
1104 layers. *Atmos. Sci. Lett.* **16**, 83–88.

1105 Taylor, J. R. 2008 *Numerical Simulations of the Stratified Oceanic Bottom Boundary Layer*.
1106 PhD thesis, University of California, San Diego.

1107 Taylor, J. R., Sarkar, S. & Armenio, V. 2005 Large eddy simulation of stably stratified
1108 open channel flow. *Phys. Fluids* **17**, 116602.

1109 Thorpe, S. A. & Liu, Z. 2009 Marginal instability? *J. Phys. Oceanogr.* **39**, 2373–2381.

1110 Turner, J. S. 1973 *Buoyancy Effects in Fluids*. Cambridge University Press.

Venayagamoorthy, S. K. & Stretch, D. D. 2010 On the turbulent Prandtl number in homogeneous stably stratified turbulence. *J. Fluid Mech.* **644**, 359–369.

Walter, R. K., Squibb, M. E., Woodson, C. B., Koseff, J. R. & Monismith, S. G. 2014 Stratified turbulence in the nearshore coastal ocean: Dynamics and evolution in the presence of internal bores. *J. Phys. Oceanogr.* **119**, 8709–8730.

Wells, M., Cenedese, C. & Caulfield, C. P. 2010 The relationship between flux coefficient and entrainment ratio in density currents. *J. Phys. Oceanogr.* **40**, 2713–2727.

Wilson, J. M. & Venayagamoorthy, S. K. 2015 A shear-based parameterization of turbulent mixing in the stable atmospheric boundary layer. *J. Atmos. Sci.* **72**, 1713–1726.

Wyngaard, J. C. 2010 *Turbulence in the Atmosphere*. Cambridge University Press.

Zhou, Q. 2015 Far-field evolution of turbulence-emitted internal waves and Reynolds number effects on a localized stratified turbulent flow. PhD thesis, Cornell University, Ithaca, New York.